Corresponding author mail id: pm685@cam.ac.uk

Cyclin D3 restricts SARS-CoV-2 Envelope incorporation into virions and interferes with viral spread.

Ravi K. Gupta[1,2,3], Petra Mlcochova[1,2,*]

1 Cambridge Institute of Therapeutic Immunology & Infectious Disease (CITIID), Cambridge, UK.
2 Department of Medicine, University of Cambridge, Cambridge, UK.
3 Africa Health Research Institute, Durban, South Africa.
* Corresponding author

Abstract

The COVID-19 pandemic caused by Severe Acute Respiratory Syndrome Coronavirus 2 (SARS-CoV-2) presents a great threat to human health. The interplay between the virus and host plays a crucial role in successful virus replication and transmission. Understanding host virus interactions is essential for development of new COVID-19 treatment strategies. Here we show that SARS-CoV-2 infection triggers redistribution of cyclin D1 and cyclin D3 from the nucleus to the cytoplasm, followed by their proteasomal degradation. No changes to other cyclins or cyclin dependent kinases were observed. Further, cyclin D depletion was independent from SARS-CoV-2-mediated cell cycle arrest in early S phase or S/G2/M phase. Cyclin D3 knockdown by small interfering RNA specifically enhanced progeny virus titres in supernatants. Finally, cyclin D3 co-immunoprecipitated with SARS-CoV-2 Envelope (E) and Membrane (M) proteins. We propose that cyclin D3 impairs efficient incorporation of Envelope protein into virions during assembly and is depleted during SARS-CoV-2 infection to restore efficient assembly and release of newly produced virions.

Keywords: assembly/cell cycle/cyclin D3/Fucci/SARS-CoV-2

Introduction

The severe acute respiratory syndrome coronavirus 2 (SARS-CoV-2) is the causative agent for the global Covid-19 pandemic. To date, SARS-CoV-2 has infected over 265 millions of people with death toll of more than 5 million people (2021). While strategies of counteracting SARS-

This article has been accepted for publication and undergone full peer review but has not been through the copyediting, typesetting, pagination and proofreading process, which may lead to differences between this version and the Version of Record. Please cite this article as doi: 10.15252/embj.2022111653

CoV-2 infection through vaccination have been partially successful, there is still a need for effective antiviral drugs given the emergence of vaccine escape variants such as Omicron. Coronaviruses, including SARS-CoV-2, like other viruses are intracellular pathogens exploiting the host cell machinery to their own advantage. The identification of cellular mechanisms and host cell targets required for SARS-CoV-2 life cycle will provide us with new knowledge that could be used to interfere with viral replication and therefore presents an alternative approach to block viral infection.

Cyclins and cyclin dependent kinases (CDKs) are the major regulators of cell cycle progression. Many viruses, including coronaviruses, adopt a strategy of manipulating cell cycle progression through cyclin-CDKs complexes (Chen & Makino, 2004; Chen *et al*, 2004; Harrison *et al*, 2007; Sun *et al*, 2018) to facilitate viral replication. Several SARS-CoV-1 proteins have been shown to reduce cyclin D and cyclin E and A expression that is connected to cell cycle arrest (Surjit *et al*, 2006; Yuan *et al*, 2006; Yuan *et al*, 2007). For example, SARS-CoV-1 N protein directly interacts with cyclin D to prolong the S phase (Surjit *et al.*, 2006) that ensure enough supply of nucleotides for viral replication. Nsp13 protein both in SARS-CoV-1 and Infectious bronchitis virus (IBV) interacts with DNA polymerase subunit to induce DNA damage and cell cycle arrest (Xu *et al*, 2011) . It is believed that the virus infection associated cell cycle arrest increases essential DNA repair processes and replication proteins that are required by virus replication.

A recent study showed that SARS-CoV-2 infection is correlated with cell arrest at S/G2 transition based on a comparison of phosphoproteomic profiles of SARS-CoV-2 infected VERO E6 cells and phosphorylation profiles collected at specific cell cycle phases. Further by measuring DNA content an increase in the fraction of cells in S and G2/M phase with decreased proportion of cells in G0/G1 phase has been observed. Additionally, kinase activity profiling uncovered that CDK1/2 activities are reduced by SARS-CoV-2, possibly adding to S/G2 phase arrest (Bouhaddou *et al*, 2020).

Here we present additional comprehensive data on SARS-CoV-2 cell cycle changes and identified cyclin D3 as a novel interactor with SARS-CoV-2 viral proteins. We propose that SARS-CoV-2 effectively reduces cyclin D3 levels in infected cells to achieve efficient viral assembly.

Results

SARS-CoV-2 infection depletes cyclin D1 and D3

Several coronaviruses are known to regulate cell cycle and cell cycle associated proteins, including cyclins (Chen & Makino, 2004; Chen *et al.*, 2004; Harrison *et al.*, 2007; Li *et al*, 2007; Yuan *et al.*, 2006; Yuan *et al.*, 2007). To determine whether the reduction in cyclins can occur during productive SARS-CoV-2 infection, the abundance of cyclins and cell cycle associated proteins (Fig 1) from SARS-CoV-2 infected cells were compared to uninfected VERO AT2 cells (Fig 1B-D) and human epithelial cell line A549 AT2 (Fig 1E,F). Western blots (Fig 1B, E) and densitometric analysis (Fig EV1A,B) indicate that cyclin D1 and D3 levels are significantly reduced compared to uninfected cells or cells infected with heat inactivated virus.

Several other cyclins tested did not show any changes in expression nor did cell cycle associated kinases that form a functional complex with cyclins and regulate together cell cycle (Fig 1A,B).

We examined the cellular distribution of cyclins D1, D3 and A2 in infected VERO AT2 cells by immunofluorescence analysis (Fig 1C, EV1C). The ratio between the fluorescence intensity of cyclins in the nucleus and cytoplasm (N/C ratio) indicates that while uninfected cells localise cyclin D1/D3 predominantly in nucleus (higher ratios), these cyclins are relocalised to the cytoplasm in infected cells (lower ratios) (Fig 1C,D,F). Importantly, cyclin A2 that was not degraded in infected cells (Fig 1B), and did not differ in cellular localisation between infected and uninfected cells. Relocation of cyclin D3 was also confirmed in HeLa cells expressing ACE2 (Fig Appendix Fig S1). Importantly, cyclin D3 degradation was confirmed in the Calu3 lung cell line endogenously expressing ACE2/TMPRSS2 (Fig EV1D).

These data indicate that a productive SARS-CoV-2 infection leads to both reduced levels of cyclin D1 and D3 and their cellular relocalisation.

Proteasome inhibition abolishes effect of SARS-CoV-2 infection on D-cyclins depletion

It is known that D-cyclins are degraded mainly through the ubiquitin dependent 26S proteasomal degradation pathway (Casanovas *et al*, 2004; Diehl *et al*, 1997). To further investigate the mechanism of D-cyclins depletion during SARS-CoV-2 infection, we investigated the involvement of proteasome degradation pathway. Cells were infected in the absence or presence of protease inhibitors MG-132 and Bortezomib and D-cyclin levels were subsequently measured (Fig 2, Appendix Fig S2). Firstly, the addition of both inhibitors before

or early after infection blocked SARS-CoV-2 infection (Appendix Fig S2A). This is in concordance with the published inhibitory effect of MG-132 on SARS-CoV-2 Mpro (Wang *et al*, 2021). In view of these results, A459 AT2 cells were infected with Delta SARS-CoV-2 variant for 24h, before addition of the proteasome inhibitor Bortezomib for an additional 24h. Uninfected cells treated with the same drug showed an increase in D-cyclin levels, suggestive of cyclin stabilization in cells. This increase was more pronounced in the case of cyclin D1 than in D3 which did not reach statistically significant levels (Fig 2A,B). Importantly, in the absence of proteasome inhibition D-cyclins relocalised from nucleus to cytoplasm and were degraded in infected cells. But proteasome inhibition significantly stabilized D-cyclins levels in infected cells where D-cyclins expression levels were equal to those in uninfected cells (Fig 2A,B, Appendix Fig S2B,C). Further, proteasome inhibition also prevented relocalisation of cyclin D3 to the cytoplasm in SARS-CoV-2 infected VERO AT2 cell (Appendix Fig S2B,C). Even though the proteasome inhibition did not completely prevent the translocation of cyclin D3 in infected A549 AT2 cells, it revealed significant presence of cyclin D3 in the nucleus (Fig 2C,D). These data indicate that the D-cyclin depletion during SARS-CoV-2 infection is mediated a proteasome-dependent pathway.

Cyclin D3 negatively regulates SARS-CoV-2 infection

To understand the functional role of D-cyclins in SARS-CoV-2 pathogenesis, the effect of cyclin knockdown on viral replication was investigated. siRNA effectively reduced levels of D and A2 cyclins by >80% at 48h post-transfection, compared to non-targeting control (NT) in A549 AT2 cells (Fig 3A, Appendix Fig S3A,B) or VERO AT2 (Fig 3C). Cells depleted for individual cyclins were infected with Delta, Alpha and WT variant to allow multiple rounds of infection (Fig 3, Appendix Fig S3). Interestingly, only viral titres from cyclin D3-depleted cells were significantly higher than those from control (NT). This was evident for all SARS-CoV-2 variants tested in both A549 AT2 and VERO AT2 cells (Fig 3B,D) and confirmed in Calu3 lung cells (Fig 3E) endogenously expressing ACE2/TMPRSS2. These data support the notion that cyclin D3 negatively modulates SARS-CoV-2 infection and could potentially have impact on viral spread.

To exclude the possibility that cyclin D3 depletion affects genomic replication, we depleted cyclin D3 in VERO AT2 cells and infected these cells with SARS-CoV-2 for 8h, allowing one round of infection and 24h, allowing multiple (~ 3) rounds of infection. RNA was isolated from cells and qPCR detecting Nucleocapsid transcripts was performed. If genome replication were affected we would expect a change in nucleocapsid transcripts in the cells, even after one round

of infection. We did not detect any differences between cells expressing and cell depleted for cyclin D3 at either 8 or 24 hours (Appendix Fig S3C).

Productive SARS-CoV-2 infection induces cell cycle arrest

Cyclin D1, D2, and D3 are important regulators of G1 to S phase progression. Given the observed depletion of cyclin D in SARS-CoV-2 infected cells we speculated that this depletion might affect cell cycle progression. Indeed, SARS-CoV-2-mediated S/G2 cell cycle arrest has been reported recently in non-human VERO E6 cells (Bouhaddou *et al.*, 2020) but its role in human cells is unknown. To understand the role between infection and D-cyclin depletion in cell cycle regulation we firstly aimed to examine previously reported cell cycle arrest phenotype. We used the FUCCI (fluorescence ubiquitination cell cycle indicator) Cell Cycle Sensor (Fig EV2) (Sakaue-Sawano *et al*, 2008) in VERO AT2 and A549 AT2 cells. VSV-G pseudotyped viral particles containing FUCCI sensor were used to transduce cells. Cells were then infected with a replication competent strain of SARS-CoV-2 for 24h, fixed and stained for nucleocapsid. Flow cytometry analysis was used to visualise G1, early S and S/G2/M phase. The FUCCI system cannot demonstrate G0 phase as it is defined as a cell population void of any fluorescent protein but cannot be differentiated from an untransduced cell population. Cells were gated on infected (expressing SARS-CoV-2 nucleocapsid) or uninfected cells with Cdt1/Geminin expression determined in both gated populations and compared (Fig 4A-D). Indeed, SARS-CoV-2 infection mediated cycle arrest in S/G2/M phase in VERO AT2 cells (Fig 4C), confirming previously published data (Bouhaddou *et al.*, 2020). Interestingly, SARS-CoV-2 mediated cell cycle arrest in A549 AT2 cells was identified specifically in early S phase (Fig 4D). This cell cycle arrest was caused by productive SARS-CoV-2 infection as use of heat inactivated virus or Remdesivir (RDV) treatment abrogated cell cycle arrest (Fig EV2D-F) and population of arrested cells increased with increasing MOI (Fig EV2G,H). All SARS-CoV-2 variants tested (WT, Alpha, Delta) caused cell cycle arrest in S/G2/M phase in VERO AT2 cells and in early S phase in A549 AT2 and (Fig 4E,F). Furthermore, cell cycle kinetics in virus exposed but uninfected cells were similar to unexposed uninfected cells (Fig EV2I,J).

These observations support the hypothesis that a productive SARS-CoV-2 infection is responsible for cell cycle arrest and that the arrest is not the result of by-stander effects.

Cell cycle arrest induced by SARS-CoV-2 is not dependent on cyclin D3 degradation

To dissect whether the increase in viral titer is a direct consequence of cylin D depletion or aftermath of cell cycle arrest caused by the absence of this cyclin, we investigated cell cycle

arrest during SARS-CoV-2 infection and linked it to cyclin D expression/cellular localization. It has been previously reported that the Cyclin D degradation is sufficient to cause cell cycle arrest in G1 phase (Agami & Bernards, 2000; Masamha & Benbrook, 2009). We confirmed cell cycle arrest in G1 phase in A549 AT2 after D-cyclin depletion (Appendix Fig S4A,B). Further VERO AT2 cells showed similar G1 arrest after individual D1 and D3 cyclin depletion but as well when both D1 and D3 cyclins were depleted together (Appendix Fig S4C). Importantly, no increase in early S nor S/G2/M phase have been observed after cyclin D depletion in uninfected cells. On the contrary, a decrease in these phases has been identified in concordance with more cells arresting in G1 phase and not progressing through the cell cycle (Appendix Fig S4). As we have already shown that SARS-CoV-2 infection increases percentage of cells in early S (in A549 AT2 cells) and S/G2/M (in VERO AT2) specific cell cycle phases (Fig 4), we investigated cell cycle progression in infected cells were D-cyclins and cyclin A had been depleted (Fig 5, EV3). A549 AT2 cells have been depleted for D and A cyclins (Fig 5A) and infected with Delta variant. The percentage of infected cells was determined 24h later and a small increase (3 fold) compare to NT control was detected in cells depleted for cyclin D3 (Fig 5B,C). The A549 AT2 cell population in early S increased without any changes in S/G2/M phase following infection in both non-targeted (NT) control cells and cells depleted for D and A cyclins (Fig 5D). This data were confirmed using an Alpha SARS-CoV-2 variant (Fig EV3A,B). Furthermore, cell cycle in virus exposed but uninfected cells showed similar cell cycle kinetics as unexposed and uninfected cells excluding any by-stander effect of infection on cell cycle changes (Fig EV3C,D). Moreover, VERO AT2 cells showed an increase in the proportion of cells in S/G2/M phase after SARS-CoV-2 infection even when D and A cyclins were depleted, confirming our results in A549 AT2 cells (Fig EV3E,F).

Importantly, SARS-CoV-2 infection still caused cell cycle arrest in early S phase in A549 AT2 even in the presence of high levels of the proteasome resistant cyclin D3 mutant (Fig 5E). Mutation at T283 prevents phosphorylation, nuclear export and proteasomal degradation (Casanovas *et al.*, 2004; Cato *et al*, 2011). Cells were transduced with lentivirus to deliver wild type (WT) cyclin D3 or mutant T283A cyclin D3, before infection with live SARS-CoV-2. Cyclin D3 could be detected in non-transduced/control cells and was completely degraded during SARS-CoV-2 infection. Cells complemented with cyclin D3 WT and T283A showed higher cyclin D3 expression than controls as expected; however after infection only WT cyclin D3 was degraded whilst T283A cyclin D3 protein persisted. Moreoever, even in the presence of high levels of T283A cyclin D3 cell cycle arrest in early S phase was clearly evident (Fig 5E). Additionally, single cell analysis showed that D-cyclins were relocated and degraded in

SARS-CoV-2 infected cells independently from cell cycle phase. VERO AT2 cells were transduced with Fucci containing lentiviral particles and 18h later infected with Delta (Fig 5F,G, EV3I) or Alpha (Fig EV3G,H) SARS-CoV-2 variant. Quantification of nuclear/cytoplasm ratio of D-cyclin staining in different cells cycle phases (identified by expression of Fucci sensor) clearly showed that cyclin D3 (Fig 5G) and cyclin D1 (Fig EV3I) in SARS-CoV-2 infected cells are relocalized from nucleus to cytoplasm probably for degradation, independent of the cell cycle phase they are in. These data suggest that cell cycle arrest induced by SARS-CoV-2 is not dependent on cyclin D3 degradation.

Cyclin D3 associates with E and M SARS-CoV-2 proteins

Cyclin D3 has been previously implicated in the restriction of influenza A virus through impairment of virus assembly (Fan *et al*, 2017). Cyclin D3 has been shown to interact with IAV protein M2, a ion channel that promotes viral replication (Fan *et al.*, 2017; Pinto & Lamb, 2006). Interestingly, SARS-CoV-2 Envelope (E) protein has been suggested to be an ion channel (Singh Tomar & Arkin, 2020; Xia *et al*, 2021). In the light of our data showing cyclin D3 depletion increased SARS-CoV-2 viral titer, we investigated potential implication of cyclin D3 in SARS-CoV-2 assembly. Firstly, the interaction between cyclin D3 and E protein was investigated using immunoprecipitation (Fig 6A). HA-tagged cyclin D3 was co-expressed together with Strep-tagged E and nsp9 protein in 293T cells. Nsp9 was chosen as a control on the basis of its diverse cellular localization both in the nucleus and cytoplasm (Zhang *et al*, 2020). Of note, 293T cells showed undetectable endogenous expression of cyclin D3 (Fig EV4A). We showed that SARS-CoV-2 Envelope (E) coimmunoprecipitated with HA-tagged cyclin D3 using anti-HA antibody while SARS-CoV-2 nsp9 protein did not (Fig 6A) suggestive of specific binding to E protein.

SARS-CoV-2 E protein is a known interactor of Membrane (M) and Nucleocapsid (N) proteins. Further, it has been shown for SARS-CoV-1 and SARS-CoV-2 that M, E and (N) structural proteins are required for efficient assembly (Kumar *et al*, 2021; Plescia *et al*, 2021; Siu *et al*, 2008; Yurkovetskiy *et al*, 2020). We expressed HA-tagged cyclin D3 with Spike (S), or Strep-tagged N, M, E, nsp9 (Fig EV4). Coimmunoprecipitation with HA-tagged cyclin D3 using anti-HA antibody or anti-cyclin D3 mouse monoclonal antibody revealed an interaction with M and E proteins (Fig EV4C,D). Further, coimmunoprecipitation using beads binding Strep-tagged protein showed pull down of HA-tagged cyclin D3 with M and E proteins (Fig EV4E). There was no evidence for binding between cyclin D3 and N or S proteins (Fig EV4). Furthermore,

Cyclin D3 interaction with M and E was confirmed by expressing cyclin D3 with E or M or both proteins together (E/M) and immunoprecipitated using anti-HA antibody (Fig 6B).

To further confirm interaction between cyclin D3 and E and M we assessed cyclin D3 effect on Spike trafficking where E and M play significant role. It has been previously reported that SARS-CoV-2 E and M proteins regulate intracellular trafficking and processing of Spike, leading to S retention in the ER and Golgi, preventing syncytia formation (Boson *et al*, 2021). It is possible that this interaction between structural proteins and spike retention allows S to target the virion assembly sites. We hypothesised that if cyclin D3 is interacting with E and M it might impact their function in Spike processing/trafficking, and we can use it as a read-out by assessing the syncytia formation.

Firstly, we confirmed that cyclin D3 degradation is independent of syncytia formation. VERO AT2 were infected with Omicron lineages BA.1 that has limited ability to form syncytia and BA.2 that is more efficient in syncytia formation (Appendix Fig S5A) (Yamasoba *et al*, 2022). Both Omicron lineages depleted cyclin D3 in cells (Appendix Fig S5B) verifying that cyclin D3 degradation is independent from syncytia formation, and also supporting the notion that cyclin D3 degradation is a conserved function among SARS-CoV-2 variants.

In the next step, a split GFP system (Cabantous *et al*, 2005) was used to confirm that E and M or combination of both (E/M) impact Spike-mediated syncytia formation as published previously (Boson *et al.*, 2021). 293T GFP11 cells were transfected with full length S (WT), and/or with E, M. 24h post-transfection cells were seeded at a 1:1 ratio with Vero-GFP10 and cell to cell fusion was measured 18h later to determine a proportion of green area to total phase area (Fig 6C-G). Indeed, both structural proteins when coexpressed with S significantly decreased GFP+ve area (cell-cell fusion) (Fig 6C,E). Interestingly, when 293T GFP11 cells were transfected with full length S (WT), and/or with E, M, and cyclin D3, cyclin D3 had no effect on reduction of syncytia when expressed together with S or S + E or S + M (Fig 6F). However, it increased syncytia formation in combination with S+M+E suggestive of compromising E and M impact on Spike processing/trafficking towards the cell surface (Fig 6D,G).

Cyclin D3 impairs Envelope incorporation into virions

To further understand the mechanism of cyclin D3 restriction during SARS-CoV-2 assembly, we used a SARS-CoV-2 viral like particle (VLP) assay. It has been shown that four SARS-CoV-2 structural proteins, Spike (S), Nucleocapsid (N), Envelope (E) and Membrane (M) are

essential for SARS-CoV-2 VLP formation. Formed VLPs have molecular and morphological properties of native virions (Syed *et al*, 2021; Xu *et al*, 2020; Yurkovetskiy *et al.*, 2020). We transfected 293T cells with plasmids encoding S,N,M,E in the presence or absence of cyclin D3 expressed from transfected plasmids. VLPs were collected in media supernatants, purified through 20% sucrose, and detected in western blot (Fig 6H-J). Even though all proteins were expressed at similar levels in cells, significantly less Envelope protein was incorporated into VLPs in the presence of cyclin D3 (Fig 6I,J). Furthermore, we noted that cyclin D3 was incorporated into VLPs as well (Fig 6I). There was no change to incorporation of Spike, M or N into virions. Suggestive of specific effect of cyclin D3 on SARS-CoV-2 Envelope protein.

Of note, Cyclin D3 has no direct effect on Spike incorporation into virions or trafficking (in the absence of E and M) as confirmed by lack of negative effect on Syncytia formation (Fig 6D,F,G), and Spike incorporation into SARS-CoV-2 VLPs (Fig 6I,J) or Spike pseudotyped HIV-1 based VLPs (Appendix Fig S5C).

Lastly, we investigated whether SARS-CoV-2 structural proteins are capable of inducing cyclin D3 degradation. We transfected 293T cells with a panel of selected SARS-CoV-2 genes. The choice of genes was based on SARS-CoV-2-human protein-protein interactions (Gordon *et al*, 2020), and based on cellular localization (e.g. nsp9, like cyclin D3, localises to the. nucleus and cytoplasm), known interaction with proteins that interact with cyclin D3 (e.g. M interacts with AKAP8L, known interactor of cyclin D3) and function that might link to proteasomal degradation in general (e.g. Orf8, binds to FBXL12, substrate-recognition component of the SCF). From 15 studied proteins, orf3b and orf10 were not expressed. Structural proteins S, N, M and E did not mediate cyclin D3 degradation (Fig EV5). Two SARS-CoV-2 proteins capable of affecting cyclin D3 expression/ degradation were identified, namely nsp1 and orf8 (Fig EV5B).

These data together demonstrate that cyclin D3 associates with M and E proteins important for SARS-CoV-2 assembly, impairing their optimal function in Spike trafficking and disrupts efficient incorporation of SARS-CoV-2 envelope into virions.

Discussion

Here we show that SARS-CoV-2 infection depletes levels of cyclin D and suggest that this depletion is independent from changes to cell cycle arrest in infected cells. Further, cyclin D3 seems to interfere with Envelope and Membrane SARS-CoV-2 protein function in Spike trafficking and E incorporation into virions.

The molecular mechanism of coronavirus-mediated regulation of cell cycle and cell cycle associated proteins has not been comprehensively investigated, especially in SARS-CoV-2 infection.

Many viruses can manipulate cell cycle of infected cells. Coronaviruses are not an exception (Chen & Makino, 2004; Chen *et al.*, 2004; Harrison *et al.*, 2007; Sun *et al.*, 2018; Surjit *et al.*, 2006; Yuan *et al.*, 2006; Yuan *et al.*, 2007). SARS-CoV-2 has been reported to arrest cell cycle in S/G2/M phase in VERO E6 cells (Bouhaddou *et al.*, 2020). Our own data confirmed this observation using the Fucci system (Koh *et al*, 2017), and comparing two different cell lines VERO AT2 (monkey, *Cercopithecus aethiops*, epithelial/kidney) and A549 AT2 (human, epithelial/lung) both expressing ACE2/TMPRSS2, we uncovered that cell cycle arrest in SARS-CoV-2 infected cells occurs at different stages of cell cycle phases. While cell cycle arrest in VERO AT2 is at late S and G2/M phase as previously reported (Bouhaddou *et al.*, 2020), A549 AT2 cell are arrested specifically at early S phase. This difference would not be possible to uncover if classical cell cycle techniques, like propidium iodine or DAPI staining, would be used as they can not separate G0 and G1 phase nor early S phase. Based on these data we can conclude that SARS-CoV-2 infection of human cells arrests the cell cycle in S phase, possibly to create a favourable environment for viral replication and spread. However, the exact mechanism is unclear at the present and warrants further investigation.

Cyclin dependent kinases (CDKs) and corresponding cyclins are essential part of cell cycle progression. Several coronaviruses have been shown to regulate these proteins (Chen & Makino, 2004; Chen *et al.*, 2004; Harrison *et al.*, 2007; Sun *et al.*, 2018; Surjit *et al.*, 2006; Yuan *et al.*, 2006; Yuan *et al.*, 2007). Specifically down-regulation of cyclin D1 has been shown in IBV (Harrison *et al.*, 2007), and SARS-CoV-1 (Surjit *et al.*, 2006), cyclin D3 reduction in SARS-CoV-1 infection (Yuan *et al.*, 2006). However, decrease in cyclin Ds has been always connected to cell cycle arrest. Here we show that SARS-CoV-2 mediate translocation of cyclin D1 and D3 from nucleus into cytoplasm for proteasome degradation in

both VERO AT2 and A549 AT2, and Calu3 cells. Analysis of other cyclins in VERO AT2 cell did not reveal any changes to cyclin A (promoting S phase entry and mitosis), B (accumulates in G2 phase), or E (limiting factor for G1 phase progression and S phase entry), supporting the notion that degradation of cyclin D proteins is specific.

Further, we present data supporting a notion that the down-regulation of cyclin D during SARS-CoV-2 infection is cell cycle arrest independent. Firstly, detailed analysis of cell cycle arrest in cells depleted for cyclin D1 and D3 revealed arrest in G1 phase as published previously (Masamha & Benbrook, 2009) not in S or G2/M phase. Nevertheless, when cells in the absence of cyclin Ds were infected, cell were still arrested in early S phase (in A549 AT2) or S/G2/M (in VERO AT2), suggestive of cell cycle arrest during infection being caused by a factor other than depletion of cyclin D proteins. Secondly, expression of proteasome resistant cyclin D3 mutant T283A had no effect on cell cycle arrest caused by SARS-CoV-2 infection. Lastly, using single cell microscopy and Fucci cell cycle sensor allowed us to measure cyclin Ds re-localization from nucleus into cytoplasm for degradation in specific cell cycle phases. All cell cycle phases detected showed that in the presence of infection cyclin Ds are always re-localized from nucleus to cytoplasm for degradation. It has been published recently that CDK1/2 activities are reduced during SARS-CoV-2 infection and might be leading to S/G2 phase arrest (Bouhaddou *et al.*, 2020). Although no changes at expression level were evident for CDKs in our study, phosphorylation state of these kinases was not investigated, and it is thus possible that such changes may occur and effect cell cycle progression.

If cyclin D is not used as a mean for virus to arrest cell cycle, it is possible that it might represent a host restriction factor preventing optimal viral replication and spread. Importantly, depletion of cyclin D3 by siRNA increased viral titres after SARS-CoV-2 infection in viral supernatants. This suggest that cyclin D3 might play role in viral spread. This effect is reminiscent of role of cyclin D3 in influenza infection, where cyclin D3 depletion resulted in increase viral production. This study also showed that cyclin D3 binds M2 protein and interferes with the M1-M2 interaction leading to defective viral assembly (Fan *et al.*, 2017).

Interestingly, M2 protein was identified as first viroporin (Duff & Ashley, 1992; Pinto *et al*, 1992). In coronaviruses several viroporins have been discovered, including SARS-CoV-1 E (Verdia-Baguena *et al*, 2012; Wilson *et al*, 2004). As E proteins are highly conserved in the SARS family, we investigated a possibility that SARS-CoV-2 Envelope and cyclin D3 are potential binding partners. Our work indeed revealed cyclin D3 as a new interactor with SARS-CoV-2 E. Recently a comparative viral-human protein-protein interaction analysis for SARS-CoV-2 have been published (Gordon *et al.*, 2020). In their study they did not uncover cyclin

D3 as an interactor with any viral protein, however, the study was conducted in HEK293T cells, cell line that we showed does not express cyclin D3. It has been shown that SARS-CoV-1 and SARS-CoV-2 proteins M, E and N are required for virion assembly that takes place in ER-Golgi intermediate compartment cisternae (Cortese *et al*, 2020; Krijnse-Locker *et al*, 1994; V'Kovski *et al*, 2021). M and E proteins seem to present an assembly core interacting with both Spike and Nucleocapsid proteins (Escors *et al*, 2001; Godeke *et al*, 2000). Importantly, our data show that cyclin D3 associates with M as well, supporting our hypothesis that cyclin D3 could impair SARS-CoV-2 assembly and/or spread. Further, E and M proteins have been implicated in Spike processing and trafficking (Boson *et al.*, 2021). We have shown that while S incorporation into particles is not affected directly by cyclin D3, trafficking of S might be altered through binding to E and/or M proteins. It has been shown that Spike is retained inside cells when expressed together with E and M probably to target S to proximity of intracellular virus assembly sites. Our data show that S is retained in the cells in the presence of M and E but its trafficking towards membrane and ability to form syncytia is partially rescued when cyclin D3 is present. This supports the concept of cyclin D3 interacting with E and M and changing their optimal function in Spike trafficking. Further, details from SARS-CoV-2 assembly assay that produces VLPs with molecular and morphological properties of native virions (Syed *et al.*, 2021; Xu *et al.*, 2020; Yurkovetskiy *et al.*, 2020), revealed that in the presence of cyclin D3, SARS-CoV-2 E is inefficiently incorporated into virions. This is an important finding as it has been shown before that SARS-CoV-1 (SARS-CoV-1 E 95% identical to SARS-CoV-2 E) virus missing E protein replicates to 100-1,000-fold lower titres than wild type, and lower viral load was accompanied by less inflammation in the lungs in a hamster model. It has been suggested that total number or virion morphology is similar, but the number of mature virions was higher in the SARS-CoV-1 infected cells than in SARS-CoV-1-ΔE infected cells (DeDiego *et al*, 2007; DeDiego *et al*, 2011). Furthermore, E proteins are known voroporins, able to form ion-conductive pores in host membranes and disrupt physiological function of cells. Viroporins are known to increase release of infectious virus from cells but also facilitate the entry of virus into cells. It has been shown that SARS-CoV-1 viruses, in which pore activity is inhibited, are less infectious and pathogenic (Nieto-Torres *et al*, 2015). It is possible that less incorporation of E in the presence of cyclin D3 into virions will have similar effect on virus as E depletion and cause changes in virus maturation and pathogenicity of SARS-CoV-2.

Surprisingly, none of SARS-CoV-2 structural proteins could degrade cyclin D3. Changes in cyclin D3 expression levels were detected in the presence of nsp1 and Orf8. nsp1 binds the

ribosomal mRNA channel to inhibit translation of both viral and native 5'UTR-containing reporter mRNA (Schubert *et al*, 2020; Wang *et al*, 2000). It is possible that actual translation of cyclin D is inhibited, but would not explain why other cyclins e.g. A2, E1 or B1 (all cyclins in this study have similarly short half-lives of 30-180min) (Penelova *et al*, 2005) are unaffected. Orf8 disrupts interferon signalling (Li *et al*, 2020), and down-regulates MHC-I in cells (Zhang *et al*, 2021), as well as regulating protein folding and transport machineries in ER (Liu *et al*, 2022). The potential role of orf8 in cyclin D3 degradation is currently not understood and is under investigation.

Our work provides important insight into mechanism through which cyclin D3 limits SARS-CoV-2 infection. In the light of immune evasion from vaccination, it is important that this phenomenon was observed across different SARS-CoV-2 variants suggesting that this mechanism provides a universal target for development of antivirals. Our data suggest that cyclin D3 associates with SARS-CoV-2 E and M proteins, decreasing E incorporation into virions and thereby interfering with efficient viral spread. SARS-CoV-2 has therefore evolved strategies to degrade cyclin D3 that require further investigation, with the hope that it can be translated to therapeutics.

Materials and Methods

Reagents

Cell lines

All cells were maintained in Dulbecco's modified Eagle medium (DMEM) supplemented with 10% fetal calf serum (FCS), 100 U ml^{-1} penicillin and 100 mg ml^{-1} streptomycin and regularly tested and found to be mycoplasma free. Following cells were a gift from: A549 ACE2/TMPRSS2 (Rihn *et al*, 2021) Massimo Palmerini, Vero ACE2/TMPRSS2 from Emma Thomson, HeLa-ACE2 from James Voss, 293T (a human embryonic kidney cell line, ATCC CRL-3216). 293T GFP11 cells and Vero-GFP10 cells for Split GFP assay were a gift from Leo James (Papa *et al*, 2021). Calu3 cells a gift from Paul Lehner, were maintained in Eagle's minimum essential medium containing 10% fetal calf serum, 1% nonessential amino acid solution, and 1% L-glutamine solution.

Viruses

WT (lineage B, SARS-CoV-2/human/Liverpool/REMRQ0001/2020), a kind gift from Ian Goodfellow, previously isolated by Lance Turtle (University of Liverpool), David Matthews and Andrew Davidson (University of Bristol). Alpha variant (B.1.1.7; SARS-CoV-2 England/ATACCC 174/2020) was a gift from G. Towers (Reuschl *et al*, 2021), lineages B.1.1.617.2 (Delta, GISAID: EPI_ISL_1731019) and B .1.1.529 (Omicron UK isolate, G. Screaton) (Dejnirattisai *et al*, 2022; Nutalai *et al*, 2022) were received as part of the work conducted by G2P-UK National Virology Consortium. Viral stocks were prepared by passaging once in VERO AT2 cells. Cells were infected at low MOI and incubated for 72h. Virus containing culture supernatants were clarified by centrifugation (500xg, 5min) and aliquots frozen at -80˚C. Standard TCID50 assay in VERO AT2 was used to determine MOI of viral stocks.

Plasmids

pBOB-EF1-FastFUCCI-Puro was a gift from Kevin Brindle & Duncan Jodrell (Addgene plasmid # 86849 ; http://n2t.net/addgene:86849 ; RRID:Addgene_86849) (Koh *et al.*, 2017). pCMV5 cyclin D3 HA was obtained from MRC-PPU Reagents and Services. Rc/CMV cyclin D1 HA was a gift from Philip Hinds (Addgene plasmid # 8948 ; http://n2t.net/addgene:8948 ;

RRID:Addgene_8948) (Baker *et al*, 2005). pLVX-EF1alpha-SARS-CoV-2-E-2xStrep-IRES-Puro (Addgene plasmid # 141385 ; http://n2t.net/addgene:141385 ; RRID:Addgene_141385); pLVX-EF1alpha-SARS-CoV-2-M-2xStrep-IRES-Puro (Addgene plasmid # 141386 ; http://n2t.net/addgene:141386 ; RRID:Addgene_141386). pLVX-EF1alpha-SARS-CoV-2-nsp9-2xStrep-IRES-Puro (Addgene plasmid # 141375 ; http://n2t.net/addgene:141375 ; RRID:Addgene_141375); pLVX-EF1alpha-SARS-CoV-2-N-2xStrep-IRES-Puro (Addgene plasmid # 141391 ; http://n2t.net/addgene:141391 ; RRID:Addgene_141391); pLVX-EF1alpha-SARS-CoV-2-orf3a-2xStrep-IRES-Puro (Addgene plasmid # 141383 ; http://n2t.net/addgene:141383 ; RRID:Addgene_141383); pLXV-EF1alpha-2xStrep-SARS-CoV-2-orf3b-IRES-Puro (Addgene plasmid # 141384 ; http://n2t.net/addgene:141384 ; RRID:Addgene_141384);pLVX-EF1alpha-SARS-CoV-2-orf7a-2xStrep-IRES-Puro (Addgene plasmid # 141388 ; http://n2t.net/addgene:141388 ; RRID:Addgene_141388); pLVX-EF1alpha-SARS-CoV-2-orf8-2xStrep-IRES-Puro (Addgene plasmid # 141390 ; http://n2t.net/addgene:141390 ; RRID:Addgene_141390); pLVX-EF1alpha-SARS-CoV-2-orf9b-2xStrep-IRES-Puro (Addgene plasmid # 141392 ; http://n2t.net/addgene:141392 ; RRID:Addgene_141392);pLXV-EF1alpha-2xStrep-SARS-CoV-2-orf9c-IRES-Puro (Addgene plasmid # 141393; http://n2t.net/addgene:141393 ; RRID:Addgene_141393); pLVX-EF1alpha-SARS-CoV-2-orf10-2xStrep-IRES-Puro (Addgene plasmid # 141394 ; http://n2t.net/addgene:141394 ; RRID:Addgene_141394); pLVX-EF1alpha-SARS-CoV-2-nsp1-2xStrep-IRES-Puro (Addgene plasmid # 141367 ; http://n2t.net/addgene:141367 ; RRID:Addgene_141367);pLVX-EF1alpha-SARS-CoV-2-nsp12-2xStrep-IRES-Puro (Addgene plasmid # 141378 ; http://n2t.net/addgene:141378 ; RRID:Addgene_141378); pLVX-EF1alpha-SARS-CoV-2-nsp13-2xStrep-IRES-Puro (Addgene plasmid # 141379 ; http://n2t.net/addgene:141379 ; RRID:Addgene_141379); pLVX-EF1alpha-eGFP-2xStrep-IRES-Puro (Addgene plasmid # 141395 ; http://n2t.net/addgene:141395 ; RRID:Addgene_141395) were a gift from Nevan Krogan (Gordon *et al.*, 2020). pEXN-MNCX, MLV vector encoding N-terminal double HA tag (Zhang *et al*, 2006). pCAGGS_SARS-CoV-2_Spike was obtained from NIBS. Plasmids used for SARS-CoV-2 assembly assay: pCov2-CoOpNucleocapsid-I-GFP, pCov2-CoOpSpike-I-GFP, pCov2-CoOpEnvelope-I-GFP, pCov2-CoOpMembrane-I-GFP were a gift from Nicholas Matheson, prepared by S. Marelli.

Antibodies

Following antibodies were used. Anti-rabbit IgG, HRP-linked Antibody (7074); Cyclin D3 Mouse mAb (DCS22, 2936); from Cell Signaling. Mouse IgG HRP Linked Whole Ab (NXA931V); from Sigma. Goat anti-Mouse IgG (H+L) Cross-Adsorbed Secondary Antibody: Alexa 488 (A-11001), Alexa 594 (A-11032), Alexa 647 (A-21236); Goat anti-Rabbit IgG (H+L) Cross-Adsorbed Secondary Antibody: Alexa 488 (A-11034), Alexa 405 (A-48254); Rabbit polyclonal SARS-CoV-2 Spike (PA1-41165); Rabbit monoclonal SARS-CoV-2 Nucleocapsid (MA5-29982) from Thermo Fisher Scientific. Mouse monoclonal Cyclin D3 (D-7, sc-6283) from Santa Cruz. Rabbit Polyclonal Cyclin A2 antibody (GTX103042); Rabbit Polyclonal Cyclin D1 antibody (N1C3, GTX108824); Rabbit Polyclonal Cyclin E1 antibody (GTX103045); Rabbit Polyclonal Cyclin B1 antibody (GTX100911); monoclonal SARS-CoV-2 Spike (GTX632604) from GeneTex. Mouse monoclonal Strep II Tag Antibody (NBP2-43735) from Novus Biologicals. Mouse monoclonal actin (ab6276) from Abcam. Strep-Tactin-HRP; MagStrep "type3" XT beads (2-4090-002) from IBA Lifesciences. Anti-HA Magnetic Beads (88836) from Thermo Fisher Scientific. Rabbit Polyclonal SARS-CoV-2 membrane glycoprotein Polyclonal Antibody (SARS-COV2-M-101AP), Rabbit Polyclonal SARS-CoV-2 envelope protein Polyclonal Antibody (SARS-COV2-E-101AP), Rabbit Polyclonal MCM2 (PA5-79645) from Thermo Fisher Scientific. Mouse monoclonal HIV-1 p24/p55 (ARP365, ARP366) from NIBSC.

SDS–PAGE and immunoblots

Cells were lysed in reducing Laemmli SDS sample buffer containing PhosSTOP (Phosphatase Inhibitor Cocktail Tablets, Roche, Switzerland) at 96°C for 10 min and the proteins separated on NuPAGE® Novex® 4–12% Bis–Tris Gels. Subsequently, the proteins were transferred onto PVDF membranes (Millipore, Billerica, MA, USA), the membranes were quenched, and proteins detected using specific antibodies. Labelled protein bands were detected using Amersham ECL Prime Western Blotting Detection Reagent (GE Healthcare, USA) and ChemiDoc MP Imaging System (Bio-Rad) CCD camera. Protein band intensities were quantified using ChemiDoc MP Imaging System and Image Lab software (Bio-Rad, Hercules, CA, USA).

Immunofluorescence

Cells were fixed in 4% PFA, quenched with 50 mM NH_4Cl and permeabilised with 0.1% Triton X-100 in PBS. After blocking in PBS/1% FCS, cells were labelled for 1 h with primary

antibodies diluted in PBS/1% FCS, washed and labelled again with Alexa Fluor secondary antibodies for 1 h. Cells were washed in PBS/1% FCS and stained with DAPI in PBS for 5 min. Labelled cells were detected using ArrayScan high-content system (ThermoFisher, Waltham, MA, USA) and analysed using Harmony (PerkinElmer, Waltham, MA, USA) and ImageJ software. Infected cells have been identified by SARS-CoV-2 Nucleocapsid or Spike staining. To measure the location of cyclin D staining in cells, DAPI staining was used to demarcate the nuclear and cytoplasmic regions of interest (ROI). Harmony (PerkinElmer, Waltham, MA, USA) and ImageJ software were used to measure MFI for each protein in each region. Values are presented as a ratio of signal (nucleus/cytoplasm). Usually, at 50-200 cells have been quantified.

Cell cycle analysis using fluorescence ubiquitination cell cycle indicator (Fucci)

Fucci cassete was cloned from pBOB-EF1-FastFucci-Puro vector to pEXN-MNCX using BamHI/NotI restriction sites. Fucci containing lentiviral particles were produced as follows. 293Tv cells were transfected with pEXN-MNCX-Fucci, CMVi and pMD2.G. Cell supernatants containing viruses (Fucci VLP) were collected 48h post-transfection and frozen at -80˚C. Cells were transduced using Fucci VLP for 18h. Cells were infected with SARS-CoV-2 variants and fixed in 4% PFA 24h post-infection. SARS-CoV-2 positive cells were identified by Nucleocapsid staining and Flow cytometry. Cell populations positive or negative for SARS-CoV-2 nucleocapsid staining were gated and Cdt1-RFP positive (G1 phase), Geminin-GFP positive (S/G2/M phase), and Cdt1-RFP/ Geminin-GFP positive (early S phase) populations were identified using flow cytometry using LSRFortessa X-20 (BD Biosciences, UK) and FlowJo software (Tree Star, OR, USA).

For immunofluorescence and high-throughput microscopy cells were transduced using Fucci VLP for 18h. Cells were infected with SARS-CoV-2 variants and fixed in 4% PFA 24h post-infection. SARS-CoV-2 positive cells were identified by Nucleocapsid or Spike staining. Cells in G1 phase were identified by Cdt1-RFP; early S, Cdt1-RFP/ Geminin-GFP; and S/G2/M, Geminin-GFP signal.

Knock-down

Cells were transfected with 20 pmol of siRNA Ambion Silencer Negative Control #1, predesigned Invitrogen Silencer siRNAs for cyclin D3 (siRNA ID s2523, Chr.6: 41934933 – 42048894), cyclin D1 (siRNA ID s229, Chr.11: 69641105 – 69654474), cyclin A2 (siRNA ID

s2514, Chr.4: 121816444 – 121823933) using Lipofectamine RNAiMAX Transfection Reagent (Invitrogen). Medium was replaced 18h post-transfection and cells infected with Delta (MOI 0.001), Alpha and WT (MOI 0.1) variant for 4h. Cells were washed twice in PBS and incubated in new medium for 48h. Cell supernatant were collected and used to determine virus titers by standart TCID50, cells were lysed and used for western blotting to detect viral and cyclins protein expression. Knock down in Calu3 cell line: Cells were transfected with 40 pmol of siRNA Ambion Silencer Negative Control #1, predesigned Invitrogen Silencer siRNAs for cyclin D3 using Lipofectamine RNAiMAX Transfection Reagent. 24h later cells were transfected again with 40 pmol of siRNA negative control or cyclin D3. Medium was replaced 48h post-transfection and cells infected with Delta (MOI 0.01) variant for 4h. Cells were washed twice in PBS and incubated in new medium for 48h. Cell supernatant were collected and used to determine virus titers by standart TCID50.

Co-immunoprecipitation

Cells were transfected with SARS-CoV-2 genes encoding full length Spike (no tag), Strep-tagged Nucleocapsid, Envelope, Membrane, nsp9 proteins in the absence/presence of HA-cyclin D3 for 24h. Cells were lysed in Pierce IP lysis buffer (ThermoFisher, Waltham, MA, USA) supplemented with protease and phosphatase inhibitor cocktail (Pierce, Rockford, IL, USA) and 1% digitonin. Cell lysates were precleared by centrifugation. A sample of whole cell lysate was stored at this point. pre-cleared cell lysates were incubated with a-HA magnetic beads, MagStrep beads (IBA-Lifescience, Gottingen, Germany) or anti-cyclin D3 monoclonal antibody (sc-xx) bound Protein G Dynabeads for 1h at 4˚C. Beads were washed 3x in IP lysis buffer and 1x in PBS. BTX elution buffer (IBA-Lifescience) was used to elute proteins from MagStrep beads. Laemmli reducing buffer was added to a-HA beads and Dynabeads and eluates from MagStrep beads and 10min at 90˚C was used to elute/denaturate attached proteins. Samples were stored till further use.

Cell to cell fusion assay

293T GFP11 cells were transfected with WT full length Spike, and/or with WT Envelope, Membrane, cyclin D3, and empty vector (pCDNA, to ensure equal amount of transfected DNA). 24h post-transfection cells were seeded at a 1:1 ratio with Vero-GFP10 cells, final cell number 6x10e4 cells/well. Cell to cell fusion was measured 18h later and determine as a proportion of green area to total phase area using ArrayScan high-content system (ThermoFisher, Waltham, MA, USA) and analysed using ImageJ software.

Spike pseudotyped lentivirus

Viral vectors were prepared by transfection of 293T cells by using Fugene HD transfection reagent (Promega) as follows. Confluent 293T cells were transfected with a mixture of 13.5ul of Fugene HD, 1µg of pCAGGS_SARS-CoV-2_Spike, 1ug of p8.91 HIV-1 gag-pol expression vector, and 1.5µg of pCSFLW (expressing the firefly luciferase reporter gene with the HIV-1 packaging signal)(Mlcochova *et al*, 2020), and 1µg pCMV5 cyclin D3 HA or 1µg of pcDNA3.1 (as a control). Viral supernatant was collected at 48h after transfection, filtered through 0.45um filter. The 50% tissue culture infectious dose ($TCID_{50}$) of SARS-CoV-2 pseudovirus was determined using Steady-Glo Luciferase assay system (Promega). Viral supernatants were centrifuged onto 25% sucrose to purify virus particles (23,000xg, 2h, 4˚C) and pellet resuspended in Laemmli reducing buffer and resolved in western blot.

SARS-CoV-2 virus like particles assembly assay

293T cell were transfected with 3ug of each plasmid encoding Spike, Nucleocapsid, Membrane, Envelope and cyclin D3 or empty plasmid (pcDNA3.1) using Fugene HD (Promega). Media and cells were collected 48h later. Media containing VLPs were filtered through 0.45µm filter and purified through 20% sucrose, at 100,000xg, 2h, 4˚C. Pellets were washed in PBS, centrifuged at 100,000xg, 2h, 4˚C. Pellets were dried overnight at 4˚C and resuspended in 2% SDS in PBS, after addition of Laemmli reducing buffer, samples were vortexed and heated at 50˚C for 20min. Western blots were performed with fresh samples immediately.

Lentiviral delivery of cyclin D3

Cyclin D3 WT and T283A mutant were cloned into to pEXN-MNCX using BamHI/NotI restriction sites. Cyclin D3 containing lentiviral particles were produced as follows. 293T cells were transfected with pEXN-MNCX-cyclin D3 (TW or T283A) CMVi and pMD2.G using Fugen HD (Promega). Cell supernatants containing viruses were collected 48h post-transfection and frozen at -80˚C.

Quantitative PCR

Total RNA was isolated from infected cellsusing Total RNA Purification Kit from Norgen Biotek (Thorold, Canada). cDNA was synthesized using Superscript III Reverse Transcriptase (Thermo Fisher Scientific) using 500ng of template RNA. qPCR was performed on QuantStudio7 (Thermo Fisher Scientific) using Fast SYRB green master mix (Thermo Fisher

Scientific). Expression levels of target genes were normalized to glyceraldehyde-3-phosphate dehydrogenase (GAPDH). Forward primer: 5'GCCTCTTCTCGTTCCTCATCAC3'; Reverse primer: 5'AGCAGCATCACCGCCATTG3'.

Data Availability

This study includes no data deposited in external repositories.

Acknowledgments

We thank Voss for HeLa ACE2; and S. Rihn for the A549-ACE2/TMPRSS2 cell, N. Matheson, and S. Marelli for full length Spike, Membrane and Envelope plasmids. This research was supported by the Cambridge NIHR BRC Cell Phenotyping Hub. In particular, we wish to thank V. Romashova for their advice and support in flow imaging. R.K.G. is supported by a Wellcome Trust Senior Fellowship in Clinical Science (WT108082AIA). We acknowledge additional support from Lister and Rosetrees Institutes.

Disclosure and competing interests statement

The authors declare no competing interests.

References

(2021) WHO Coronavirus (COVID-19) Dashboard. *https://covid19whoint/*

Agami R, Bernards R (2000) Distinct initiation and maintenance mechanisms cooperate to induce G1 cell cycle arrest in response to DNA damage. *Cell* 102: 55-66

Baker GL, Landis MW, Hinds PW (2005) Multiple functions of D-type cyclins can antagonize pRb-mediated suppression of proliferation. *Cell Cycle* 4: 330-338

Boson B, Legros V, Zhou B, Siret E, Mathieu C, Cosset FL, Lavillette D, Denolly S (2021) The SARS-CoV-2 envelope and membrane proteins modulate maturation and retention of the spike protein, allowing assembly of virus-like particles. *J Biol Chem* 296: 100111

Bouhaddou M, Memon D, Meyer B, White KM, Rezelj VV, Marrero MC, Polacco BJ, Melnyk JE, Ulferts S, Kaake RM *et al* (2020) The Global Phosphorylation Landscape of SARS-CoV-2 Infection. *Cell* 182: 685-+

Cabantous S, Terwilliger TC, Waldo GS (2005) Protein tagging and detection with engineered self-assembling fragments of green fluorescent protein. *Nat Biotechnol* 23: 102-107

Casanovas O, Jaumot M, Paules AB, Agell N, Bachs O (2004) P38SAPK2 phosphorylates cyclin D3 at Thr-283 and targets it for proteasomal degradation. *Oncogene* 23: 7537-7544

Cato MH, Chintalapati SK, Yau IW, Omori SA, Rickert RC (2011) Cyclin D3 is selectively required for proliferative expansion of germinal center B cells. *Mol Cell Biol* 31: 127-137

Chen CJ, Makino S (2004) Murine coronavirus replication induces cell cycle arrest in G0/G1 phase. *J Virol* 78: 5658-5669

Chen CJ, Sugiyama K, Kubo H, Huang C, Makino S (2004) Murine coronavirus nonstructural protein p28 arrests cell cycle in G0/G1 phase. *J Virol* 78: 10410-10419

Cortese M, Lee JY, Cerikan B, Neufeldt CJ, Oorschot VMJ, Kohrer S, Hennies J, Schieber NL, Ronchi P, Mizzon G *et al* (2020) Integrative Imaging Reveals SARS-CoV-2-Induced Reshaping of Subcellular Morphologies. *Cell Host Microbe* 28: 853-866 e855

DeDiego ML, Alvarez E, Almazan F, Rejas MT, Lamirande E, Roberts A, Shieh WJ, Zaki SR, Subbarao K, Enjuanes L (2007) A severe acute respiratory syndrome coronavirus that lacks the E gene is attenuated in vitro and in vivo. *J Virol* 81: 1701-1713

DeDiego ML, Nieto-Torres JL, Jimenez-Guardeno JM, Regla-Nava JA, Alvarez E, Oliveros JC, Zhao J, Fett C, Perlman S, Enjuanes L (2011) Severe acute respiratory syndrome coronavirus envelope protein regulates cell stress response and apoptosis. *PLoS Pathog* 7: e1002315

Dejnirattisai W, Huo J, Zhou D, Zahradnik J, Supasa P, Liu C, Duyvesteyn HME, Ginn HM, Mentzer AJ, Tuekprakhon A *et al* (2022) SARS-CoV-2 Omicron-B.1.1.529 leads to widespread escape from neutralizing antibody responses. *Cell* 185: 467-484 e415

Diehl JA, Zindy F, Sherr CJ (1997) Inhibition of cyclin D1 phosphorylation on threonine-286 prevents its rapid degradation via the ubiquitin-proteasome pathway. *Genes Dev* 11: 957-972

Duff KC, Ashley RH (1992) The transmembrane domain of influenza A M2 protein forms amantadine-sensitive proton channels in planar lipid bilayers. *Virology* 190: 485-489

Escors D, Ortego J, Laude H, Enjuanes L (2001) The membrane M protein carboxy terminus binds to transmissible gastroenteritis coronavirus core and contributes to core stability. *J Virol* 75: 1312-1324

Fan Y, Mok CK, Chan MC, Zhang Y, Nal B, Kien F, Bruzzone R, Sanyal S (2017) Cell Cycle-independent Role of Cyclin D3 in Host Restriction of Influenza Virus Infection. *J Biol Chem* 292: 5070-5088

Godeke GJ, de Haan CA, Rossen JW, Vennema H, Rottier PJ (2000) Assembly of spikes into coronavirus particles is mediated by the carboxy-terminal domain of the spike protein. *J Virol* 74: 1566-1571

Gordon DE, Hiatt J, Bouhaddou M, Rezelj VV, Ulferts S, Braberg H, Jureka AS, Obernier K, Guo JZ, Batra J *et al* (2020) Comparative host-coronavirus protein interaction networks reveal pan-viral disease mechanisms. *Science* 370

Harrison SM, Dove BK, Rothwell L, Kaiser P, Tarpey I, Brooks G, Hiscox JA (2007) Characterisation of cyclin D1 down-regulation in coronavirus infected cells. *FEBS Lett* 581: 1275-1286

Koh SB, Mascalchi P, Rodriguez E, Lin Y, Jodrell DI, Richards FM, Lyons SK (2017) A quantitative FastFUCCI assay defines cell cycle dynamics at a single-cell level. *J Cell Sci* 130: 512-520

Krijnse-Locker J, Ericsson M, Rottier PJ, Griffiths G (1994) Characterization of the budding compartment of mouse hepatitis virus: evidence that transport from the RER to the Golgi complex requires only one vesicular transport step. *J Cell Biol* 124: 55-70

Kumar B, Hawkins GM, Kicmal T, Qing E, Timm E, Gallagher T (2021) Assembly and Entry of Severe Acute Respiratory Syndrome Coronavirus 2 (SARS-CoV2): Evaluation Using Virus-Like Particles. *Cells* 10

Li FQ, Tam JP, Liu DX (2007) Cell cycle arrest and apoptosis induced by the coronavirus infectious bronchitis virus in the absence of p53. *Virology* 365: 435-445

Li JY, Liao CH, Wang Q, Tan YJ, Luo R, Qiu Y, Ge XY (2020) The ORF6, ORF8 and nucleocapsid proteins of SARS-CoV-2 inhibit type I interferon signaling pathway. *Virus Res* 286: 198074

Liu P, Wang X, Sun Y, Zhao H, Cheng F, Wang J, Yang F, Hu J, Zhang H, Wang CC *et al* (2022) SARS-CoV-2 ORF8 reshapes the ER through forming mixed disulfides with ER oxidoreductases. *Redox Biol* 54: 102388

Masamha CP, Benbrook DM (2009) Cyclin D1 degradation is sufficient to induce G1 cell cycle arrest despite constitutive expression of cyclin E2 in ovarian cancer cells. *Cancer Res* 69: 6565-6572

Mlcochova P, Collier D, Ritchie A, Assennato SM, Hosmillo M, Goel N, Meng B, Chatterjee K, Mendoza V, Temperton N *et al* (2020) Combined Point-of-Care Nucleic Acid and Antibody Testing for SARS-CoV-2 following Emergence of D614G Spike Variant. *Cell Rep Med* 1: 100099

Nieto-Torres JL, Verdia-Baguena C, Jimenez-Guardeno JM, Regla-Nava JA, Castano-Rodriguez C, Fernandez-Delgado R, Torres J, Aguilella VM, Enjuanes L (2015) Severe acute respiratory syndrome coronavirus E protein transports calcium ions and activates the NLRP3 inflammasome. *Virology* 485: 330-339

Nutalai R, Zhou D, Tuekprakhon A, Ginn HM, Supasa P, Liu C, Huo J, Mentzer AJ, Duyvesteyn HME, Dijokaite-Guraliuc A *et al* (2022) Potent cross-reactive antibodies following Omicron breakthrough in vaccinees. *Cell* 185: 2116-2131 e2118

Papa G, Mallery DL, Albecka A, Welch LG, Cattin-Ortola J, Luptak J, Paul D, McMahon HT, Goodfellow IG, Carter A *et al* (2021) Furin cleavage of SARS-CoV-2 Spike promotes but is not essential for infection and cell-cell fusion. *PLoS Pathog* 17: e1009246

Penelova A, Richman L, Neupert B, Simanis V, Kuhn LC (2005) Analysis of the contribution of changes in mRNA stability to the changes in steady-state levels of cyclin mRNA in the mammalian cell cycle. *FEBS J* 272: 5217-5229

Pinto LH, Holsinger LJ, Lamb RA (1992) Influenza virus M2 protein has ion channel activity. *Cell* 69: 517-528

Pinto LH, Lamb RA (2006) The M2 proton channels of influenza A and B viruses. *J Biol Chem* 281: 8997-9000

Plescia CB, David EA, Patra D, Sengupta R, Amiar S, Su Y, Stahelin RV (2021) SARS-CoV-2 viral budding and entry can be modeled using BSL-2 level virus-like particles. *J Biol Chem* 296: 100103

Reuschl AK, Thorne LG, Zuliani-Alvarez L, Bouhaddou M, Obernier K, Hiatt J, Soucheray M, Turner J, Fabius JM, Nguyen GT *et al* (2021) Host-directed therapies against early-lineage SARS-CoV-2 retain efficacy against B.1.1.7 variant. *bioRxiv*

Rihn SJ, Merits A, Bakshi S, Turnbull ML, Wickenhagen A, Alexander AJT, Baillie C, Brennan B, Brown F, Brunker K *et al* (2021) A plasmid DNA-launched SARS-CoV-2 reverse genetics system and coronavirus toolkit for COVID-19 research. *PLoS Biol* 19: e3001091

Sakaue-Sawano A, Kurokawa H, Morimura T, Hanyu A, Hama H, Osawa H, Kashiwagi S, Fukami K, Miyata T, Miyoshi H *et al* (2008) Visualizing spatiotemporal dynamics of multicellular cell-cycle progression. *Cell* 132: 487-498

Schubert K, Karousis ED, Jomaa A, Scaiola A, Echeverria B, Gurzeler LA, Leibundgut M, Thiel V, Muhlemann O, Ban N (2020) Author Correction: SARS-CoV-2 Nsp1 binds the ribosomal mRNA channel to inhibit translation. *Nat Struct Mol Biol* 27: 1094

Singh Tomar PP, Arkin IT (2020) SARS-CoV-2 E protein is a potential ion channel that can be inhibited by Gliclazide and Memantine. *Biochem Biophys Res Commun* 530: 10-14

Siu YL, Teoh KT, Lo J, Chan CM, Kien F, Escriou N, Tsao SW, Nicholls JM, Altmeyer R, Peiris JS *et al* (2008) The M, E, and N structural proteins of the severe acute respiratory syndrome coronavirus are required for efficient assembly, trafficking, and release of virus-like particles. *J Virol* 82: 11318-11330

Sun P, Wu H, Huang J, Xu Y, Yang F, Zhang Q, Xu X (2018) Porcine epidemic diarrhea virus through p53-dependent pathway causes cell cycle arrest in the G0/G1 phase. *Virus Res* 253: 1-11

Surjit M, Liu B, Chow VT, Lal SK (2006) The nucleocapsid protein of severe acute respiratory syndrome-coronavirus inhibits the activity of cyclin-cyclin-dependent kinase complex and blocks S phase progression in mammalian cells. *J Biol Chem* 281: 10669-10681

Syed AM, Taha TY, Tabata T, Chen IP, Ciling A, Khalid MM, Sreekumar B, Chen PY, Hayashi JM, Soczek KM *et al* (2021) Rapid assessment of SARS-CoV-2 evolved variants using virus-like particles. *Science*: eabl6184

V'Kovski P, Kratzel A, Steiner S, Stalder H, Thiel V (2021) Coronavirus biology and replication: implications for SARS-CoV-2. *Nat Rev Microbiol* 19: 155-170

Verdia-Baguena C, Nieto-Torres JL, Alcaraz A, DeDiego ML, Torres J, Aguilella VM, Enjuanes L (2012) Coronavirus E protein forms ion channels with functionally and structurally-involved membrane lipids. *Virology* 432: 485-494

Wang W, Caldwell MC, Lin S, Furneaux H, Gorospe M (2000) HuR regulates cyclin A and cyclin B1 mRNA stability during cell proliferation. *EMBO J* 19: 2340-2350

Wang Z, Zhao Y, Wang Q, Xing Y, Feng L, Kong J, Peng C, Zhang L, Yang H, Lu M (2021) Identification of proteasome and caspase inhibitors targeting SARS-CoV-2 M(pro). *Signal Transduct Target Ther* 6: 214

Wilson L, McKinlay C, Gage P, Ewart G (2004) SARS coronavirus E protein forms cation-selective ion channels. *Virology* 330: 322-331

Xia B, Shen X, He Y, Pan X, Liu FL, Wang Y, Yang F, Fang S, Wu Y, Duan Z *et al* (2021) SARS-CoV-2 envelope protein causes acute respiratory distress syndrome (ARDS)-like pathological damages and constitutes an antiviral target. *Cell Res* 31: 847-860

Xu LH, Huang M, Fang SG, Liu DX (2011) Coronavirus infection induces DNA replication stress partly through interaction of its nonstructural protein 13 with the p125 subunit of DNA polymerase delta. *J Biol Chem* 286: 39546-39559

Xu R, Shi M, Li J, Song P, Li N (2020) Construction of SARS-CoV-2 Virus-Like Particles by Mammalian Expression System. *Front Bioeng Biotechnol* 8: 862

Yamasoba D, Kimura I, Nasser H, Morioka Y, Nao N, Ito J, Uriu K, Tsuda M, Zahradnik J, Shirakawa K *et al* (2022) Virological characteristics of the SARS-CoV-2 Omicron BA.2 spike. *Cell* 185: 2103-2115 e2119

Yuan X, Wu J, Shan Y, Yao Z, Dong B, Chen B, Zhao Z, Wang S, Chen J, Cong Y (2006) SARS coronavirus 7a protein blocks cell cycle progression at G0/G1 phase via the cyclin D3/pRb pathway. *Virology* 346: 74-85

Yuan X, Yao Z, Wu J, Zhou Y, Shan Y, Dong B, Zhao Z, Hua P, Chen J, Cong Y (2007) G1 phase cell cycle arrest induced by SARS-CoV 3a protein via the cyclin D3/pRb pathway. *Am J Respir Cell Mol Biol* 37: 9-19

Yurkovetskiy L, Wang X, Pascal KE, Tomkins-Tinch C, Nyalile TP, Wang Y, Baum A, Diehl WE, Dauphin A, Carbone C *et al* (2020) Structural and Functional Analysis of the D614G SARS-CoV-2 Spike Protein Variant. *Cell* 183: 739-751 e738

Zhang F, Hatziioannou T, Perez-Caballero D, Derse D, Bieniasz PD (2006) Antiretroviral potential of human tripartite motif-5 and related proteins. *Virology* 353: 396-409

Zhang J, Cruz-Cosme R, Zhuang MW, Liu D, Liu Y, Teng S, Wang PH, Tang Q (2020) A systemic and molecular study of subcellular localization of SARS-CoV-2 proteins. *Signal Transduct Target Ther* 5: 269

Zhang Y, Chen Y, Li Y, Huang F, Luo B, Yuan Y, Xia B, Ma X, Yang T, Yu F *et al* (2021) The ORF8 protein of SARS-CoV-2 mediates immune evasion through down-regulating MHC-Iota. *Proc Natl Acad Sci U S A* 118

Figure legend

Figure 1

SARS-CoV-2 infection depletes cyclin D1 and D3

(A) Diagram of cell cycle and cyclin expression during cell cycle. Cyclins drive cell cycle changes by interacting with cyclin dependent kinases (CDK).

(B-C) VERO AT2 cells were infected with WT and alpha (α) SARS-CoV-2 live virus variants, and heat inactivated α variant at MOI 0.1. (B) Cells were lysed 48h post-infection and viral protein as well as cell cycle associated protein expression was analysed by western blot. N, nucleocapsid. (C) VERO AT2 Cells were fixed 24h post-infection and stained for viral proteins and cyclins. Arrowheads highlight un-infected cells and cyclin D/A nuclear localization. Arrowheads: Nuclear cyclin staining in uninfected cells. Scale bars: 20μm.

(D) VERO AT2 cells. Quantification of cyclin A2, D1 and D3 relocalization from nucleus after infection. Uninfected (-) and SARS-CoV-2 infected cells were identified by negative/positive nucleocapsid or Spike staining. Ratio between nuclear and cytoplasm staining intensity of cyclins was measured using ImageJ and Harmony (PerkinElmer). At least 50 cells were counted. Bars indicate mean with SD. Statistical analysis was performed using two-sided unpaired Student's t-tests; ns, non-significant; $^{****}p < 0.0001$.

(E) A549 AT2 cells were infected with WT, alpha (α), and delta (Δ) SARS-CoV-2 variants. Cells were lysed 48h post-infection and viral, cyclin proteins expression was analysed by western blot. N, nucleocapsid.

(F) A549 AT2 cells. Quantification of cyclin A2, D1 and D3 relocalization from nucleus after infection. Uninfected (-) and SARS-CoV-2 infected cells were identified by negative/positive nucleocapsid or Spike staining. Ratio between nuclear and cytoplasm (N/C ratio) staining intensity of cyclins was measured using ImageJ and Harmony (PerkinElmer). At least 50 cells were counted. Bars indicate mean with SD. Statistical analysis was performed using two-sided unpaired Student's t-tests; ns, non-significant; $^{***}p < 0.001$; $^{****}p < 0.0001$.

Figure 2

Proteasome inhibition abolishes effect of SARS-CoV-2 infection on D-cyclins depletion

(A) A549 AT2 cells were infected with Delta SARS-CoV-2 variant. Proteasome inhibitor Bortezomib (BZ, 1μM) was added to cells 18h post-infection. Cells were lysed 24h post-

addition of inhibitor and cyclins and viral proteins were detected by western blot. (N) nucleocapsid.

(B) Densitometry analysis of western blots for D-cyclins (normalized to actin) in A549 AT2 cells. Plots are average of 2 (cyclin D1), 3 (cyclin D3) biological replicates. Bars indicate mean with SD. Statistical analysis was performed using ordinary two way ANOVA; ns, non-significant; $^{*}p < 0.1$.

(C) A459 AT2 cells were infected with Delta SARS-CoV-2 variant. Proteasome inhibitor Bortezomib (BZ, 1μM) was added to cells 8h post-infection. Cells were fixed and stained 24h post-addition of inhibitor. (N) nucleocapsid.Scale bars: 40μm. Contour lines represent outlines of infected cells.

(D) Quantification of D3 cyclin relocalization from nucleus after infection. Uninfected (-) and SARS-CoV-2 infected cells were identified by negative/positive nucleocapsid staining. Ratio between nuclear and cytoplasm (N/C ratio) staining intensity of cyclins was measured using ImageJ and Harmony (PerkinElmer). At least 50 cells have been counted. Bars indicate mean with SD. Statistical analysis was performed using ordinary two-way ANOVA; $^{***}p < 0.001$.

Figure 3

Cyclin D3 impairs SARS-CoV-2 spreading infection

(A-D) (A,B) D and A-cyclins were depleted using siRNA in A549 AT2 cells. Cells were infected 18h later with Delta (Δ), Alpha (α) or wild type (WT) SARS-CoV-2 variants at MOI 0.001, 0.1, 0.1 respectively. Cells were washed 4h post-infection and new media were added. Supernatants and cells were collected 48h later for western blots (A) and TCID50 (B). (C,D) D and A-cyclins were depleted using siRNA in VERO AT2 cells. Cells were infected 18h later with Alpha (α) or wild type (WT) SARS-CoV-2 variants at MOI 0.1. Cells were washed 4h post-infection and new media added. Supernatants and cells were collected at 24h and 48h later. (A,C) Representative example of western blot from uninfected cell lysates collected at 72h post-knockdown. (B,D) Virus titres in cell culture supernatants were determined as TCID50 in VERO AT2 cells.

(E) Cyclin D3 was depleted using siRNA in Calu3 cells. Cells were infected 48h later with Delta SARS-CoV-2 at MOI 0.01. Cells were washed 4h post-infection and new media were added. Supernatants and cells were collected 48h later for western blot and TCID50. Uninfected cell lysates were used for western blot.

Data information: Graphs represent average of n=3 (B,D); n=4 (E) biological replicates. Statistical analysis was performed using one-way ANOVA with Dunnett's multiple comparisons test. NT, non-targeting control. ns, non-significant; *p < 0.1; **p < 0.01; ***p < 0.001. Bars indicate mean with SD.

Figure 4

SARS-CoV-2 infection arrests cell cycle

Cells were transduced with Fucci containing lentiviral particles for 18h and infected with SARS-CoV-2 variants for additional 24h.

(A, B) (A) VERO AT2 or (B) A549 AT2 cells. Example of gating strategy for cell cycle analysis. The population of cells exposed to SARS-CoV-2 was stained for nucleocapsid (N) protein and gated on N+ve and N-ve population. Cells were further analysed for expression of cdt1 and Geminin. See also Supplemental Figure S5.

(C, D) (C) VERO AT2 or (D) A549 AT2 cells infected with WT SARS-CoV-2. Quantification of Cdt1 +ve cells (G1), Cdt1/Geminin +ve cells (early S phase) and Geminin +ve cells (S,G2,M phase) cells. n = 4 biological replicates; one-way ANOVA with Dunnett's multiple comparisons test: ns, non-significant; *p < 0.1; ***p < 0.001; ****p < 0.0001. Bars indicate mean with SD.

(E, F) (E) VERO AT2 or (F) A549 AT2 cells. Quantification of cell cycle arrest after exposure of cells to SARS-CoV-2 variants. α, alpha (MOI 0.5); Δ, delta (MOI 0.1); WT, Wuhan (MOI 0.5). n = 4 biological replicates; one-way ANOVA with Dunnett's multiple comparisons test: ns, non-significant; ****p < 0.0001; ***p < 0.001. Bars indicate mean with SD.

Figure 5

SARS-CoV-2 mediated depletion of D-cyclins is cell cycle arrest independent

(A-D) A549 AT2 cells were depleted for D and A2 cyclins and 18h later infected with Delta variant SARS-CoV-2 for 24h. Cells were fixed, stained for SARS-CoV-2 nucleocapsid and analysed for infection and Fucci cell cycle sensor. (A) A representative western blot from lysates of uninfected knock-down cells. (B) Example of gating strategy for flow cytometry analysis. (C) Percentage of infected cells in cells depleted for cyclins. n=3 biological replicates; Ordinary two-way ANOVA with Sidak's multiple comparisons test: ns, non-significant; ****p < 0.0001; **p < 0.01; *p < 0.1. Bars indicate mean with SD. (D) Flow cytometry analysis of early S and S/G2/M cell cycle phases comparing cyclin D1, D3, and A2 knockdown to NT (non-

target siRNA). n = 3-4 biological replicates. Statistical analysis was performed using two-sided unpaired Student's t-tests; ns, non-significant; $^{**}p < 0.01$; $^{*}p < 0.1$. Bars indicate mean with SD.

(E) A549 AT2 cells were transduced with VSV-G pseudotyped Fucci containing lentiviral particles and VSV-G pseudotyped lentiviral particles containing WT cyclin D3 or T283A mutant cyclin D3 (mutant not degraded by proteasome). Cells were infected 24h later and collected 48h post-infection for flow cytometry analysis of early S and western blot. n=2 biological replicates; Ordinary two-way ANOVA with Sidak's multiple comparisons test: ns, non-significant; $^{**}p < 0.01$. Bars indicate mean with SD.

(F,G) VERO AT2 cells were transduced with VSV-G pseudotyped Fucci containing lentiviral particles and 18h later infected with Delta variant SARS-CoV-2. Cells were fixed and stained for D-cyclins 24h later. (F) Example of acquisition using automated microscopic platform. Cells are identified for infection, expression of cyclin D3, and cell cycle (Red/arrow=G1phase; Green/arrowhead=S/G2/M; Red+Green/arrowhead=early S). Scale bar: 20μm. (G) Quantification of D-cyclins re-localization from nucleus to cytoplasm and correlation with cell cycle phases using ImageJ and Harmony (PerkinElmer). At least 50-200 cells were analysed in each condition. Bars indicate mean with SD. Statistical analysis was performed using two-sided unpaired Student's t-tests; $^{*}p < 0.1$.

Figure 6

Cyclin D3 associates with SARS-CoV-2 protein E and M

(A) 293T cells were contransfected with HA - cyclin D3 and Strep-tag-SARS-CoV-2 E or nsp9, and control plasmid (EV). Immunoprecipitation was performed using anti-HA antibody. The immunoprecipitates were blotted with anti-Strep, anti-HA, and cyclin D3 antibodies.

(B) 293T cells were contransfected with HA - cyclin D3 and Strep-tag-SARS-CoV-2 E, M, both E and M or nsp9. Immunoprecipitation was performed using anti-HA antibody. The immunoprecipitates were blotted with anti-Strep, anti-HA antibodies. WCL, whole cell lysate.

(C-G) 293T GFP11 cells were transfected with Spike, and/or with Envelope, Membrane, and cyclin D3. 24h post-transfection cells were seeded at a 1:1 ratio with Vero-GFP10 cells and percentage of GFP+ve area (syncytia) were determined 18h later. S, Spike; E, Envelope; M, Membrane; D3, cyclin D3.

(C,D) Representative images of GFP+ syncytia. Scale bars: 40μm.

(E-G) Quantification of cell-to-cell fusion showing percentage of the GFP+ve area to the acquired total cell area. (E) n=4 biological replicates. (F,G) n = 4 biological replicates;

technical triplicates shown; one-way ANOVA with Dunnett's multiple comparisons test: ns, non-significant; $^{****}p < 0.0001$; $^{***}p < 0.001$; $^{**}p < 0.01$. Bars indicate mean with SD.

(H) Diagram of SARS-CoV-2 VLPs construction in the presence or absence of cyclin D3 in 293T cells.

(I) Representative example of western blot from purified SARS-CoV-2 Virus Like Particles (VLPs) and whole cell lysates (WCL). MCM2 was used as loading control.

(J) Quantification of protein incorporation (into VLPs) or expression (in WCL). n = 4 biological replicates; one-way ANOVA with Dunnett's multiple comparisons test: ns, non-significant; $^{***}p < 0.001$. Bars indicate mean with SD. N, nucleocapsid; M, membrane; E, envelope; S, spike.

Expanded View Figures

EV1

Densitometry data from cell lysates from SARS-CoV-2 infected cells

(A,B) ImageJ was used to record densitometry of bands from Figure 1A,D. All band densities were normalised to actin and further normalised to uninfected cells (=1). (A) VERO AT2 cell line. (B) A549 AT2 cell line.

(C) VERO AT2 cells were infected with alpha (α) SARS-CoV-2 variant. Cells were fixed 24h post-infection and stained for viral proteins and cyclins. Arrowheads highlight un-infected cells and cyclin D/A nuclear localization. Arrowheads: Nuclear cyclin staining in uninfected cells.Scale bars: 20μm.

(D) Calu3 cells were infected with alpha (α), and delta (Δ) SARS-CoV-2 variants at MOI 0.1. Cells were lysed 8, 24 and 48h post-infection and viral proteins and cyclin D3 expression was analysed by western blot. N, nucleocapsid.

EV2

SARS-CoV-2 infection of VERO AT2 arrests cells in S and G2/M phases

(A) FUCCI (fluorescence ubiquitination cell cycle indicator) Cell Cycle Sensor is a two-color (red and green) indicator. Red: RFP-Cdt1 protein is expressed in G1 phase. GFP-Geminin protein is expressed in S, G2 and M phase. Both proteins are expressed in early S phase (both red and green colour).

(B) Cell cycle analysis can be performed using flow cytometry. G0/neg population of cells can not be analysed as it comprises of cells that are in G0 phase and/or were not transduced by Fucci containing lentiviral particles.

(C) Automated microscope platform and ImageJ and/or Harmony imaging software (PerkinElmer) analysis can be used to study Cell cycle changes. Scale bar: 20μm.

(D-F) (D) VERO AT2 cells were transduced with Fucci containing lentiviral particles for 18h and infected with SARS-CoV-2 WT in the absence (-) or presence of Chloroquine (CQ), Remdesivir (RVD) or infected with heat inactivated virus for additional 24h. % infected cells was determined by staining of SARS-CoV-2 nucleocapsid (NP) in infected cells using flow cytometry. (E) Western blot for SARS-CoV-2 Spike protein as a measure of infection in cells. (F) Analysis of cell cycle phases. n = 3 biological replicates; Statistical analysis was performed using two-sided unpaired Student's t-tests; ns, non-significant; $^{***}p < 0.001$; $^{**}p < 0.01$. Bars indicate mean with SD.

(G,H) VERO AT2 cells were transduced with Fucci containing lentiviral particles for 18h and infected with SARS-CoV-2 WT at different MOI for 24h. (G) Cells were lysed and used for Western blot. (H) Cells and their cell cycle status were analysed using Flow cytometry. n = 3 biological replicates; one-way ANOVA with Dunnett's multiple comparisons test: $^{***}p < 0.001$; $^{**}p < 0.01$. Bars indicate mean with SD.

(I-J) A549 AT2 cells were transduced with Fucci containing lentiviral particles for 18h and infected with SARS-CoV-2 variants for additional 24h. Comparison of uninfected cell populations from truly uninfected cells (not exposed to virus, uninfected) and cells exposed to SARS-CoV-2 but uninfected (Nucleocapsid negative, uninfected (INF)) or infected (Nucleocapsid positive). (I) Example of gating strategy for cell cycle analysis. (J) Quantification of cell cycle arrest in early S phase after exposure of SARS-CoV-2 variants. α, alpha; Δ, delta; WT, Wuhan. n = 3 biological replicates; two-way ANOVA test: ns, non-significant; $^{****}p < 0.0001$; $^{***}p < 0.001$; $^{**}p < 0.01$. Bars indicate mean with SD.

EV3

SARS-CoV-2 mediated depletion of D-cyclins is cell cycle arrest independent

(A-D) A549 AT2 cells were depleted for D and A2 cyclins and 18h later infected with Alpha variant SARS-CoV-2 for 24h. Cells were fixed, stained for SARS-CoV-2 nucleocapsid and analysed for infection and Fucci cell cycle sensor. (A) Percentage of infected cells in cells depleted for cyclins. n=2 biological replicates. Bars indicate mean with SD. (B) Flow

cytometry analysis of early S cell cycle phase comparing cyclin D1, D3, and A2 knockdown to NT (non-target siRNA) in two independent experiments in duplicates. Statistical analysis was performed using two-sided unpaired Student's t-tests; ns, non-significant; ***p < 0.001; **p < 0.01; *p < 0.1. Bars indicate mean with SD. (C,D) Comparison of uninfected cell populations from truly uninfected cells (not exposed to virus, uninfected) and cells exposed to SARS-CoV-2 but uninfected (Nucleocapsid negative, uninfected (INF)). A549 AT2 cells were transduced with Fucci containing lentiviral particles for 18h and infected with (C) Alpha and (D) Delta SARS-CoV-2 variants for additional 24h. n = 3 biological replicates. Statistical analysis was performed using two-sided unpaired Student's t-test: ns, non-significant. Bars indicate mean with SD.

(E-I) VERO AT2 cells were transduced with VSV-G pseudotyped Fucci containing lentiviral particles and 18h later infected with Alpha SARS-CoV-2. Cells were fixed and stained for SARS-CoV-2 nucleocapsid, D-cyclins and analysed for infection and Fucci cell cycle sensor 24h later. Statistical analysis was performed using two-sided unpaired Student's t-tests; ns, non-significant. Bars indicate mean with SD. (E) VERO AT2 cells infected with Alpha variant. Flow cytometry analysis of cell cycle comparing cyclin D1, D3, combined D1+D3 knockdown to NT (non-target siRNA) in uninfected and SARS-CoV-2 infected cells. Plot is an example of 3 biological replicates, in technical duplicates. Statistical analysis was performed using two-sided unpaired Student's t-test: ns, non-significant; ****p < 0.0001. Bars indicate mean with SD. (F) VERO AT2 cells infected with Delta variant. Flow cytometry analysis of S/G2/M cell cycle phase comparing cyclin D3 knockdown to NT (non-target siRNA). n = 3 biological replicates. Statistical analysis was performed using two-sided unpaired Student's t-test: ns, non-significant; **p < 0.01. Bars indicate mean with SD. (G) Example of acquisition using automated microscopic platform. Cells are identified for infection, cell cycle (Red/arrow=G1phase; Green/arrowhead=S/G2/M; Red+Green/arrowhead=early S) and expression of cyclin D3. Scale bar: 20μm. (H,I) Quantification of cyclin D3 re-localization from nucleus to cytoplasm and correlation with cell cycle phases using ImageJ and Harmony (PerkinElmer). (H) Cyclin D3. (I) Cyclin D1. At least 50-200 cells were analysed in each condition. Bars indicate mean with SD. Statistical analysis was performed using two-sided unpaired Student's t-test: ****p < 0.0001; ***p < 0.001.

EV4

Cyclin D3 associates with E and M proteins

(A) Western blot of cell lysates from cell lines used in this study, detecting endogenous expression of cyclin D1, D3.

(B) 293T cells were contransfected with HA-cyclin D3 and SARS-CoV-2 Spike, or Strep-tagged E, M, N or nsp9. Whole Cell lysates show expression levels of protein input into immunoprecipitation.

(C-E) Immunoprecipitation was performed using (C) mouse anti-cyclin D3 antibody, (D) anti-HA antibody, E) anti-Strep beads. The immunoprecipitates were blotted and stained with anti-Strep, anti-HA, and anti-Spike antibodies. *non-specific band. N, nucleocapsid; E, envelope; M, membrane; S, spike.

EV5

Envelope and Membrane proteins are not responsible for cyclin D degradation.

293T cells were co-transfected with SARS-CoV-2 genes (tagged with Strep-Tag) and cyclin D3.

(A) Cell lysates were collected 24h post-transfection and subjected to western blotting.

(B) Cyclin D3 expression/degradation was quantified as cyclin D3 band intensity, normalised to actin. n=5 biological replicates; ordinary one way ANOVA with Dunnett's multiple comparisons test: $^{***}p < 0.001$; $^{*}p < 0.1$. Bars indicate mean with SD.

(C,D) Examples of 2 independent experiments demonstrating experimental variation. EV, empty vector; GFP, Strep-tagged GFP expressed.

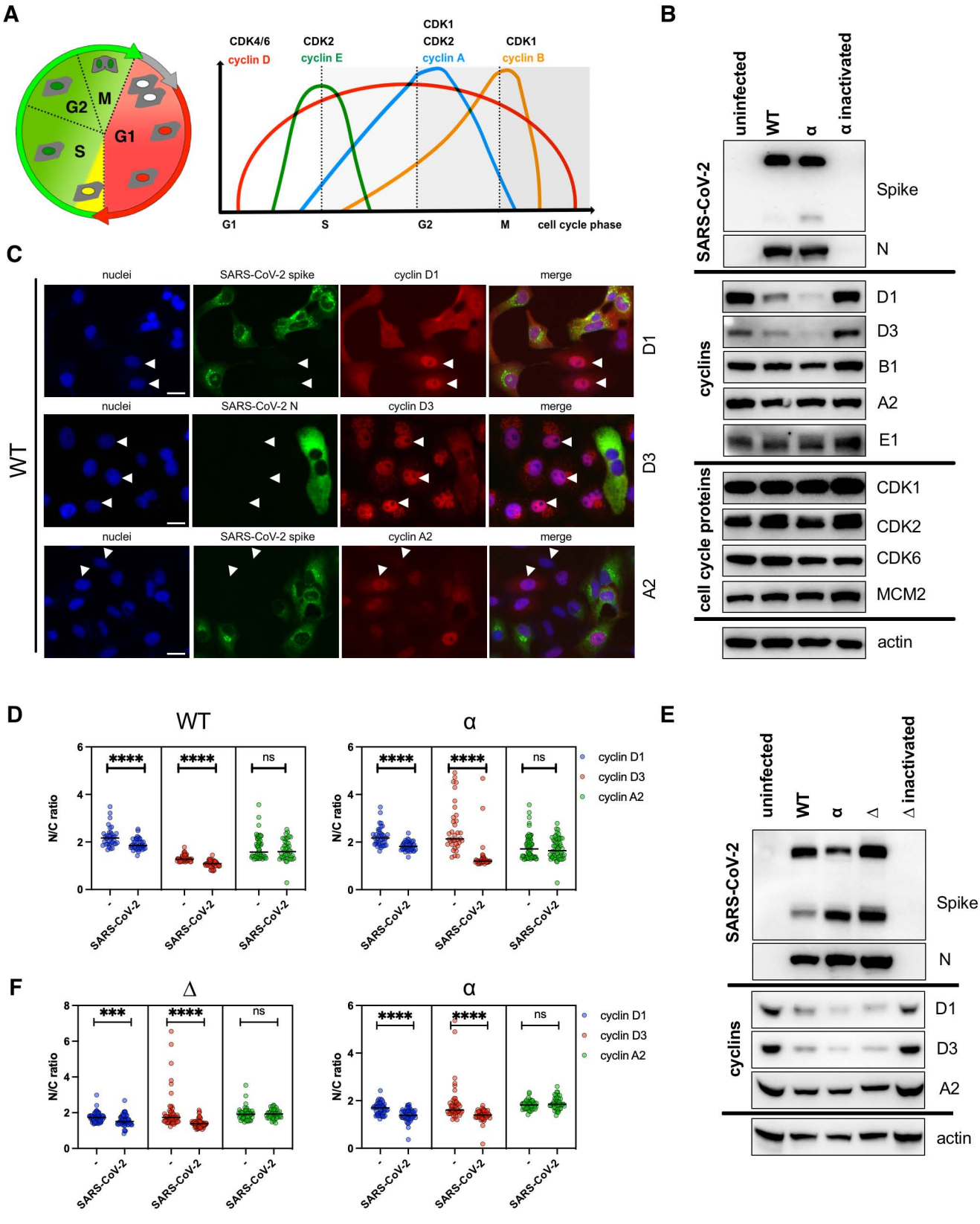
A
G2
M
G1
S
CDK4/6
cyclin D
CDK2
cyclin E
CDK1
CDK2
cyclin A
CDK1
cyclin B
G1
S
G2
M
cell cycle phase
B
uninfected
WT
α
α inactivated
SARS-CoV-2
Spike
N
cyclins
D1
D3
B1
A2
E1
cell cycle proteins
CDK1
CDK2
CDK6
MCM2
actin
C
WT
nuclei
SARS-CoV-2 spike
cyclin D1
merge
D1
nuclei
SARS-CoV-2 N
cyclin D3
merge
D3
nuclei
SARS-CoV-2 spike
cyclin A2
merge
A2
D
WT
α
N/C ratio
****
****
ns
cyclin D1
cyclin D3
cyclin A2
-
SARS-CoV-2
E
uninfected
WT
α
Δ
Δ inactivated
SARS-CoV-2
Spike
N
cyclins
D1
D3
A2
actin
F
Δ
α
N/C ratio
***
****
ns
cyclin D1
cyclin D3
cyclin A2
SARS-CoV-2

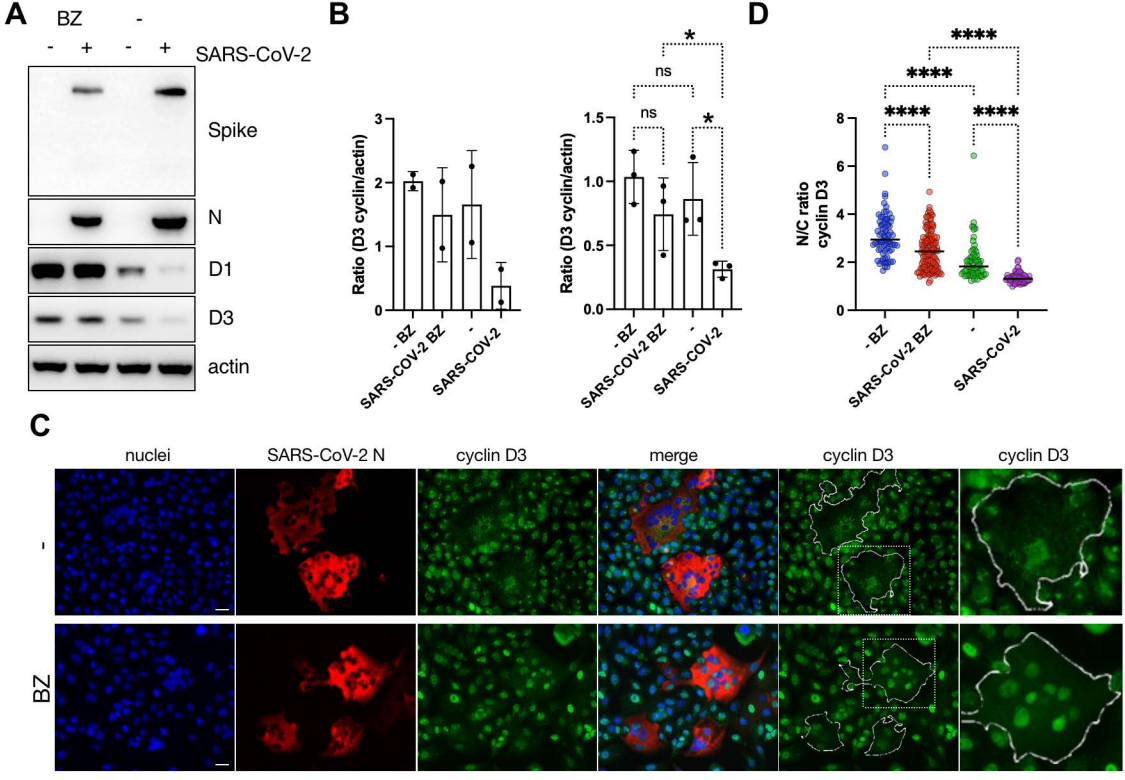
A
BZ
-
- + - +
SARS-CoV-2
Spike
N
D1
D3
actin
B
Ratio (D3 cyclin/actin)
- BZ
SARS-COV-2 BZ
-
SARS-COV-2
ns
*
ns
*
D
N/C ratio cyclin D3
****
****
****
****
C
nuclei
SARS-CoV-2 N
cyclin D3
merge
cyclin D3
cyclin D3
-
BZ

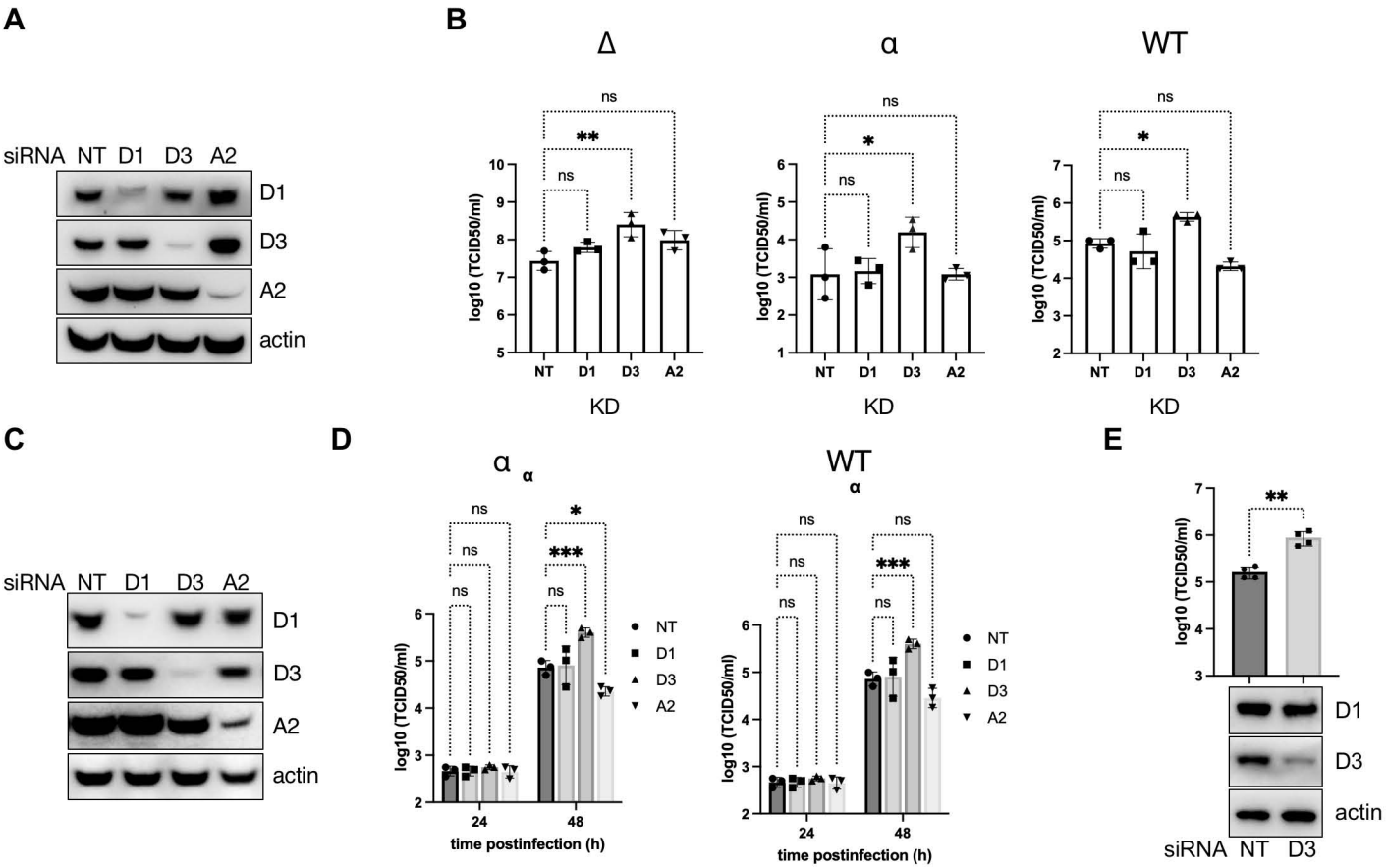
A
siRNA NT D1 D3 A2
D1
D3
A2
actin
B
Δ
α
WT
log10 (TCID50/ml)
ns
**
*
NT D1 D3 A2
KD
C
siRNA NT D1 D3 A2
D1
D3
A2
actin
D
α
α
WT
α
log10 (TCID50/ml)
ns
*
***
NT
D1
D3
A2
24
48
time postinfection (h)
E
log10 (TCID50/ml)
**
D1
D3
actin
siRNA NT D3

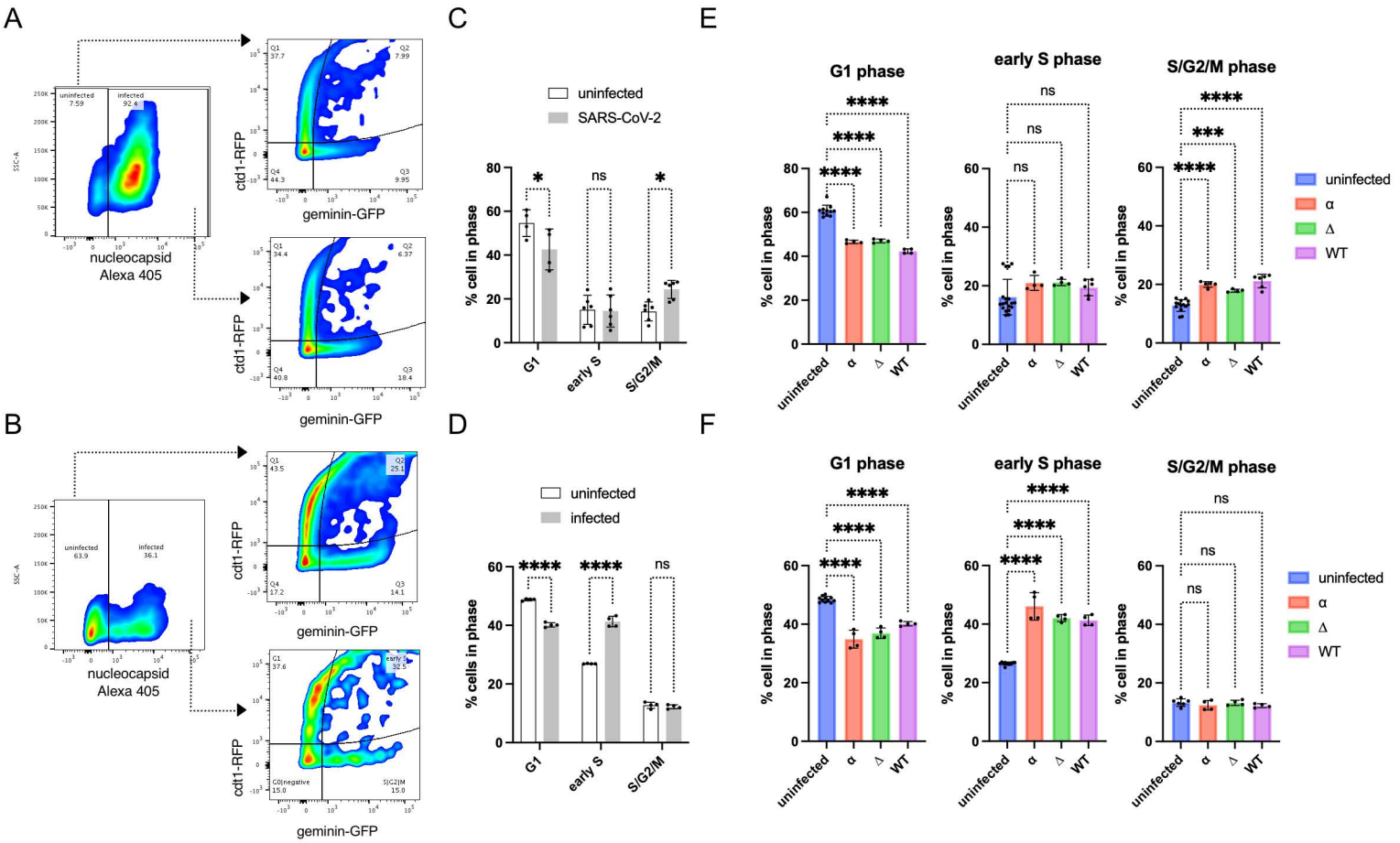
A
B
C
D
E
F
uninfected
infected
SARS-CoV-2
nucleocapsid
Alexa 405
ctd1-RFP
geminin-GFP
% cell in phase
% cells in phase
G1
early S
S/G2/M
G1 phase
early S phase
S/G2/M phase
α
Δ
WT

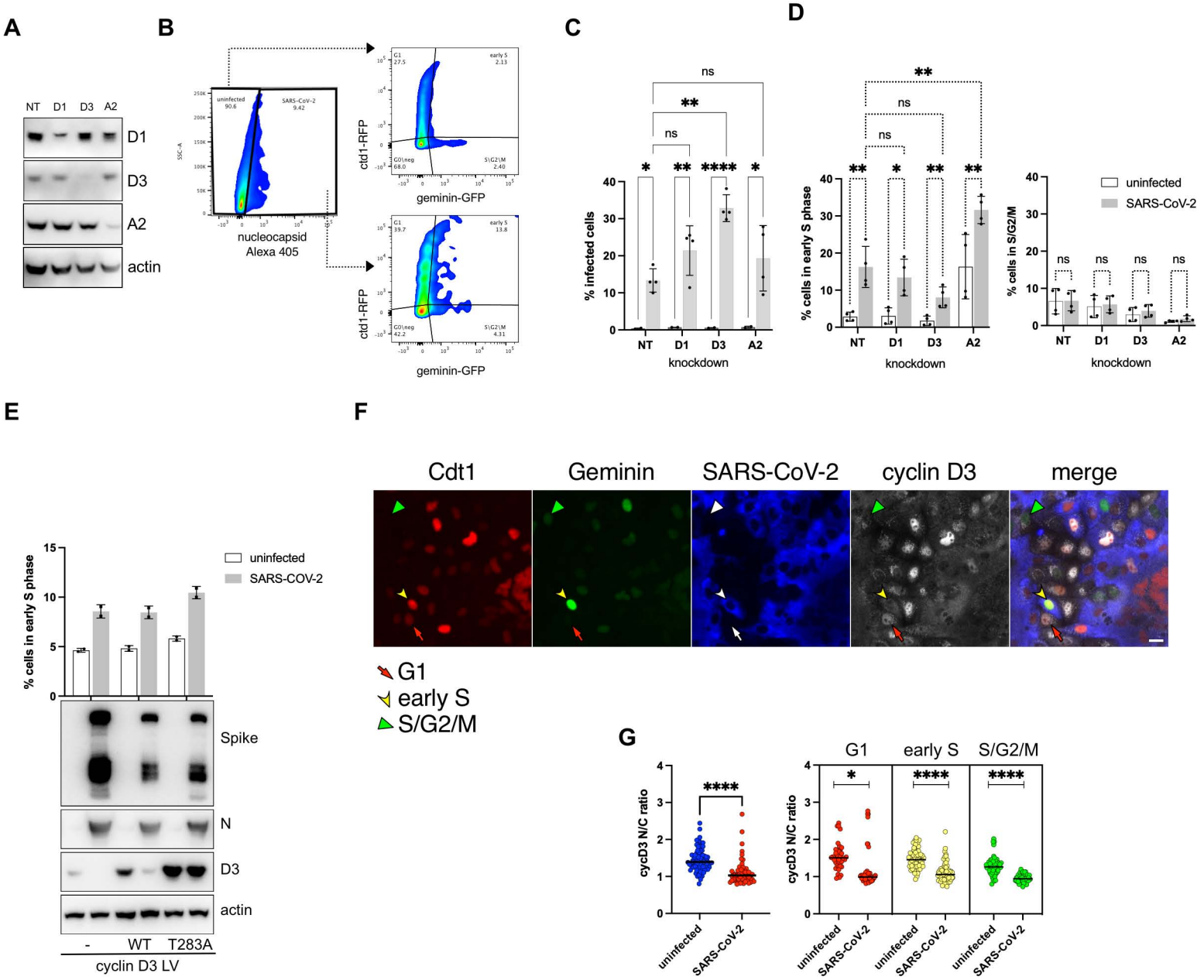
A
NT D1 D3 A2
D1
D3
A2
actin
B
uninfected
SARS-CoV-2
nucleocapsid
Alexa 405
cfd1-RFP
geminin-GFP
C
% infected cells
knockdown
NT D1 D3 A2
D
% cells in early S phase
% cells in S/G2/M
uninfected
SARS-CoV-2
E
% cells in early S phase
Spike
N
D3
actin
- WT T283A
cyclin D3 LV
F
Cdt1
Geminin
SARS-CoV-2
cyclin D3
merge
G1
early S
S/G2/M
G
cycD3 N/C ratio
G1
early S
S/G2/M

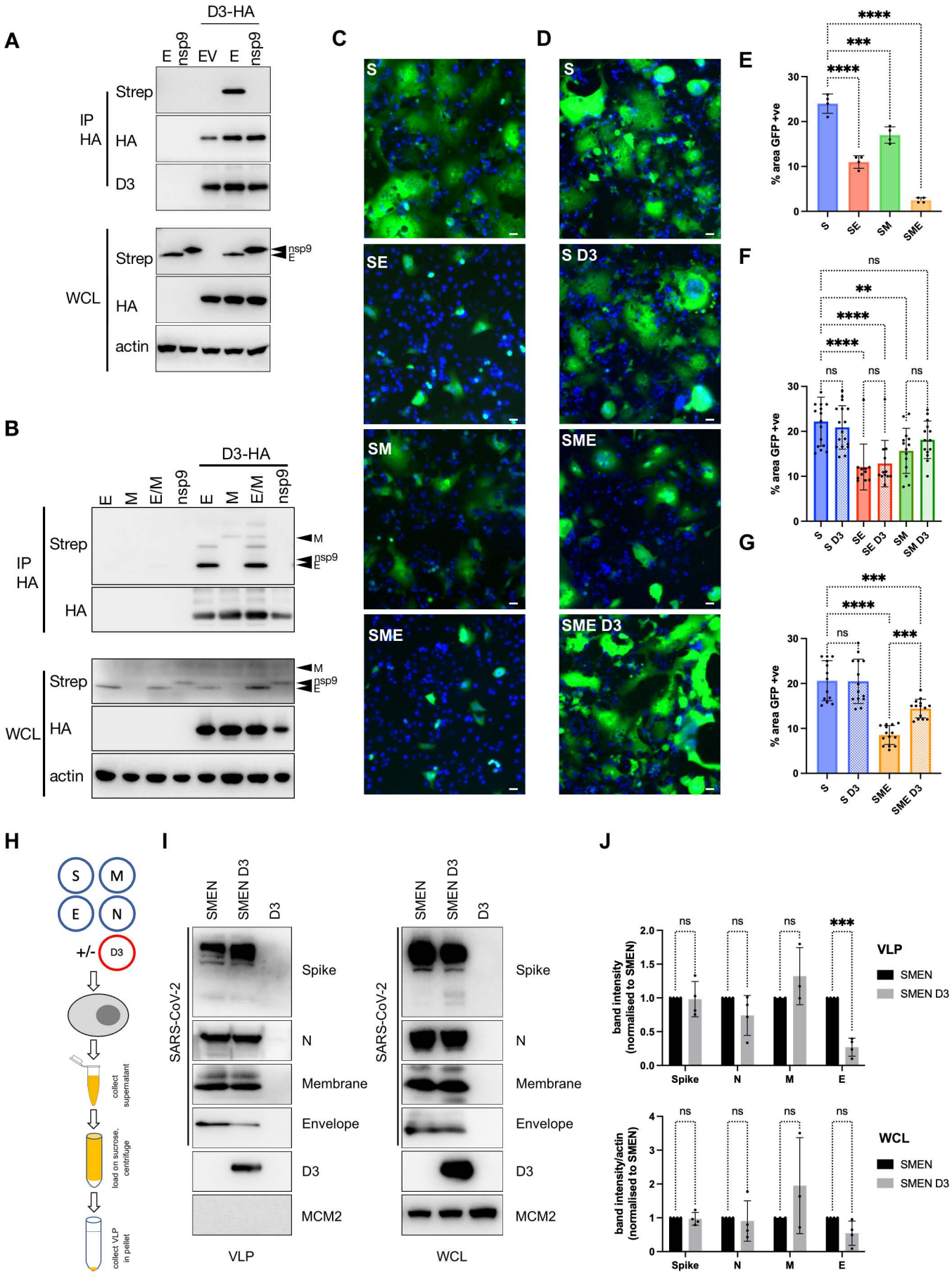
A
D3-HA
E
nsp9
EV
E
nsp9
IP
HA
Strep
HA
D3
WCL
Strep
HA
actin
nsp9
E
B
D3-HA
E
M
E/M
nsp9
E
M
E/M
nsp9
IP
HA
Strep
HA
M
nsp9
E
WCL
Strep
HA
actin
M
nsp9
E
C
S
SE
SM
SME
D
S
S D3
SME
SME D3
E
% area GFP +ve
S
SE
SM
SME
F
% area GFP +ve
S
S D3
SE
SE D3
SM
SM D3
G
% area GFP +ve
S
S D3
SME
SME D3
H
S
M
E
N
+/-
D3
collect supernatant
load on sucrose, centrifuge
collect VLP in pellet
I
SMEN
SMEN D3
D3
SARS-CoV-2
Spike
N
Membrane
Envelope
D3
MCM2
VLP
WCL
J
band intensity (normalised to SMEN)
Spike
N
M
E
VLP
SMEN
SMEN D3
band intensity/actin (normalised to SMEN)
WCL
SMEN
SMEN D3

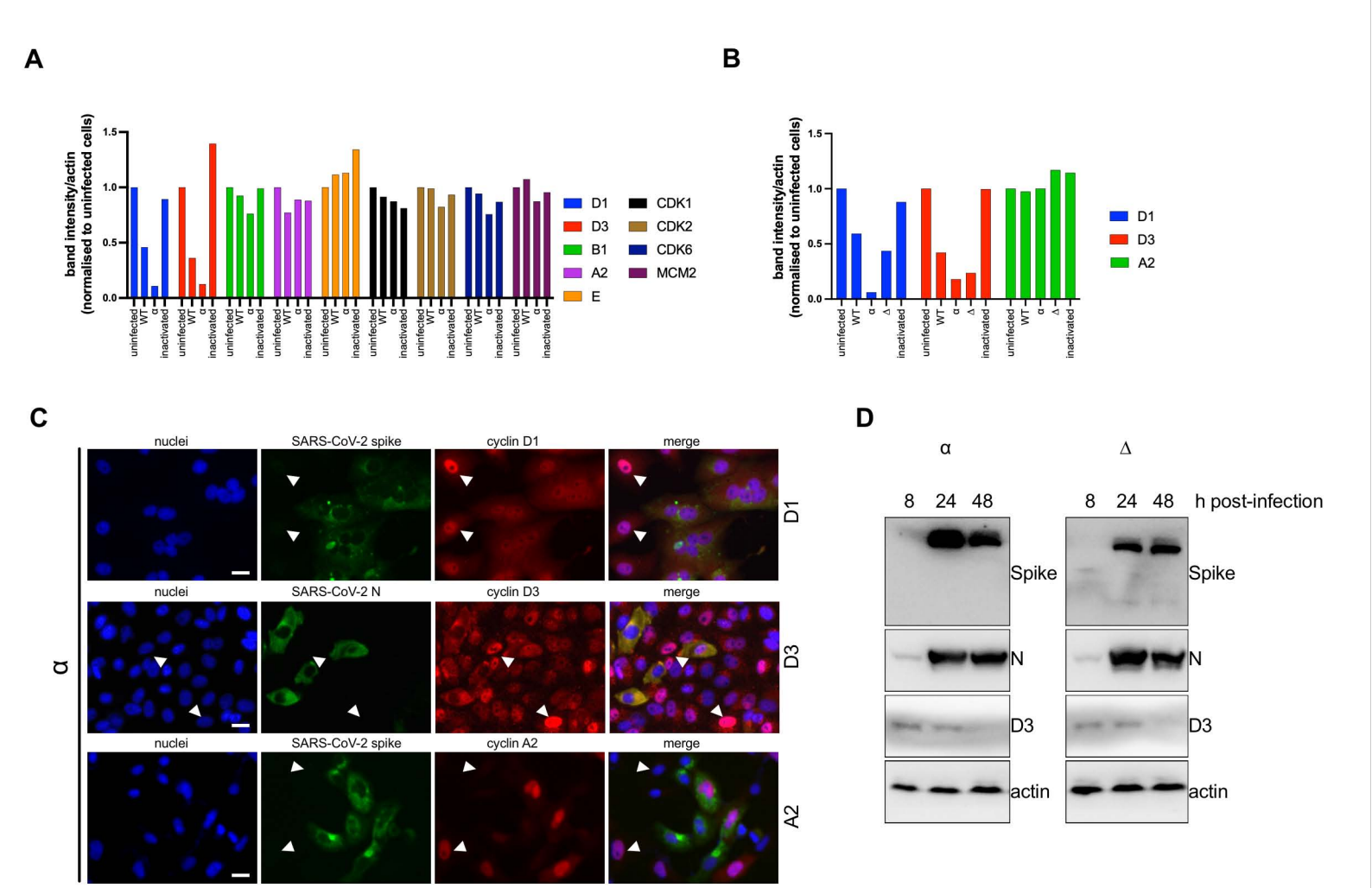
A
band intensity/actin
(normalised to uninfected cells)
1.5
1.0
0.5
0.0
uninfected
WT
α
inactivated
D1
D3
B1
A2
E
CDK1
CDK2
CDK6
MCM2
B
band intensity/actin
(normalised to uninfected cells)
uninfected
WT
α
Δ
inactivated
D1
D3
A2
C
α
nuclei
SARS-CoV-2 spike
cyclin D1
merge
D1
nuclei
SARS-CoV-2 N
cyclin D3
merge
D3
nuclei
SARS-CoV-2 spike
cyclin A2
merge
A2
D
α
Δ
8
24
48
h post-infection
Spike
N
D3
actin

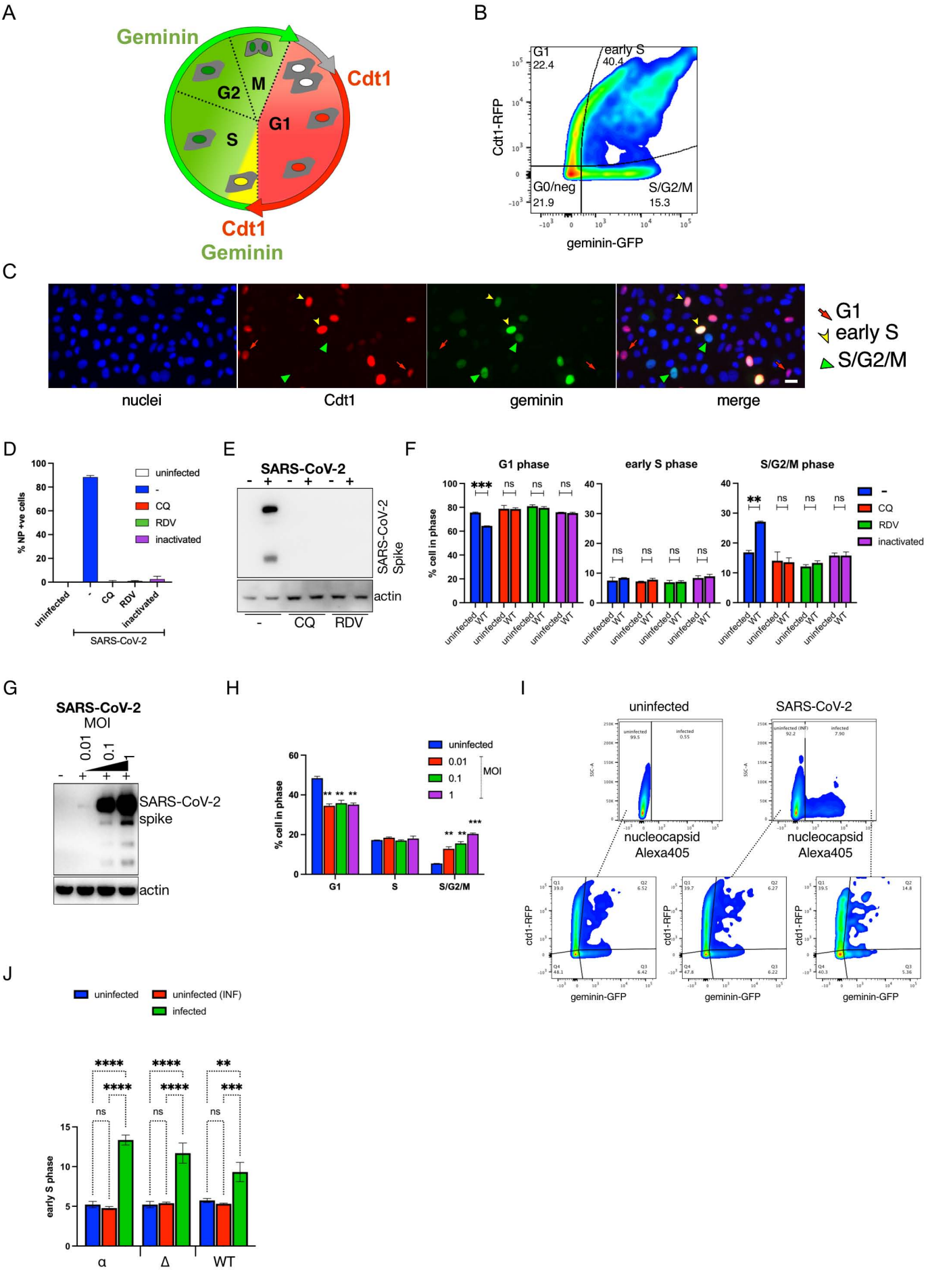
A
Geminin
Cdt1
G2
M
G1
S
Cdt1
Geminin
B
G1
22.4
early S
40.4
G0/neg
21.9
S/G2/M
15.3
Cdt1-RFP
geminin-GFP
C
G1
early S
S/G2/M
nuclei
Cdt1
geminin
merge
D
% NP +ve cells
uninfected
-
CQ
RDV
inactivated
SARS-CoV-2
E
SARS-CoV-2
SARS-CoV-2 Spike
actin
-
CQ
RDV
F
G1 phase
early S phase
S/G2/M phase
% cell in phase
***
**
ns
uninfected
WT
-
CQ
RDV
inactivated
G
SARS-CoV-2
MOI
0.01
0.1
1
SARS-CoV-2 spike
actin
H
% cell in phase
uninfected
0.01
0.1
1
MOI
G1
S
S/G2/M
I
uninfected
SARS-CoV-2
nucleocapsid Alexa405
ctd1-RFP
geminin-GFP
J
uninfected
uninfected (INF)
infected
early S phase
****
***
**
ns
α
Δ
WT

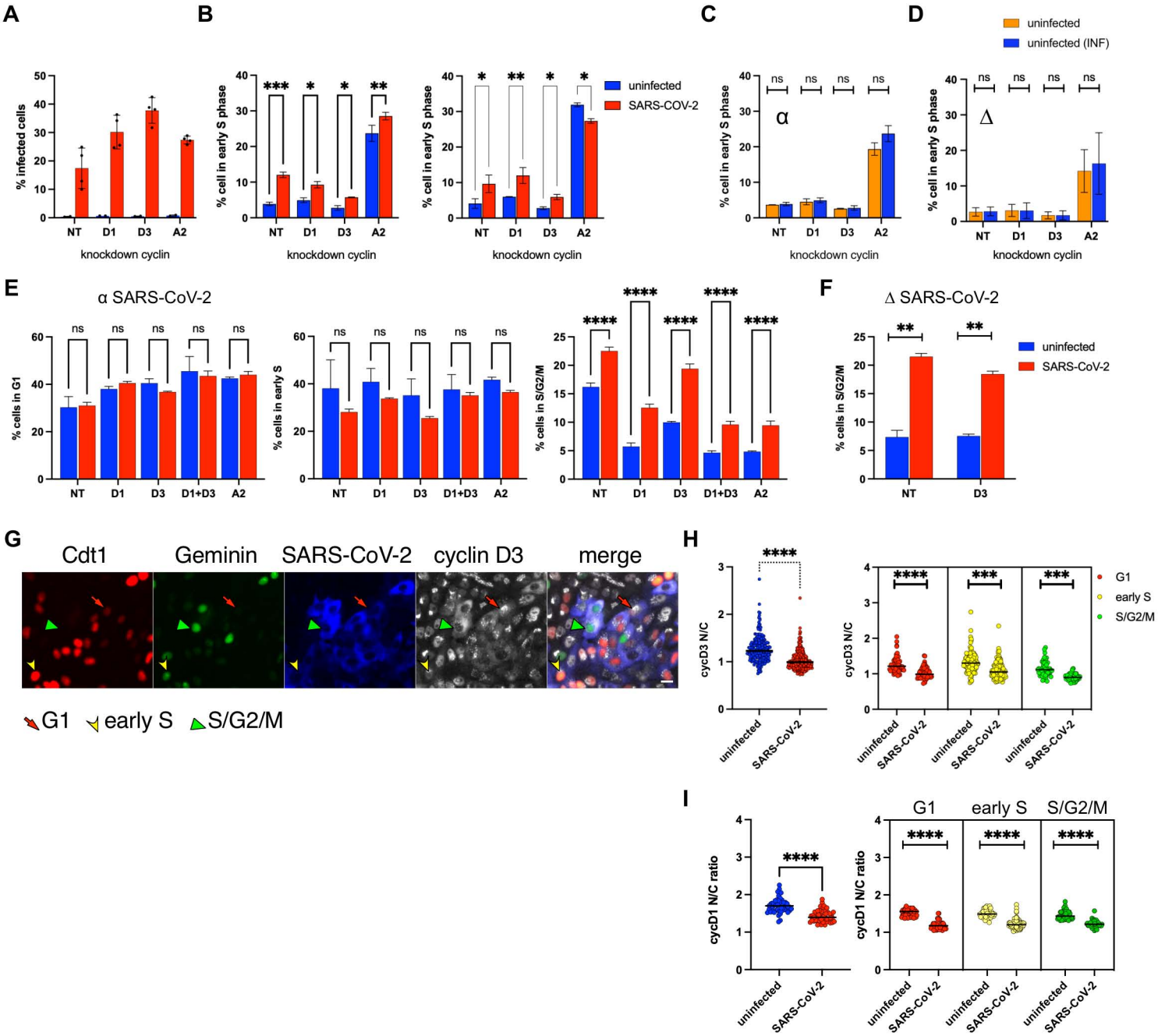
A
B
C
D
% infected cells
% cell in early S phase
knockdown cyclin
NT
D1
D3
A2
uninfected
SARS-COV-2
uninfected (INF)
α
Δ
ns
E
α SARS-CoV-2
% cells in G1
% cells in early S
% cells in S/G2/M
D1+D3
F
Δ SARS-CoV-2
G
Cdt1
Geminin
SARS-CoV-2
cyclin D3
merge
G1
early S
S/G2/M
H
cycD3 N/C
I
cycD1 N/C ratio

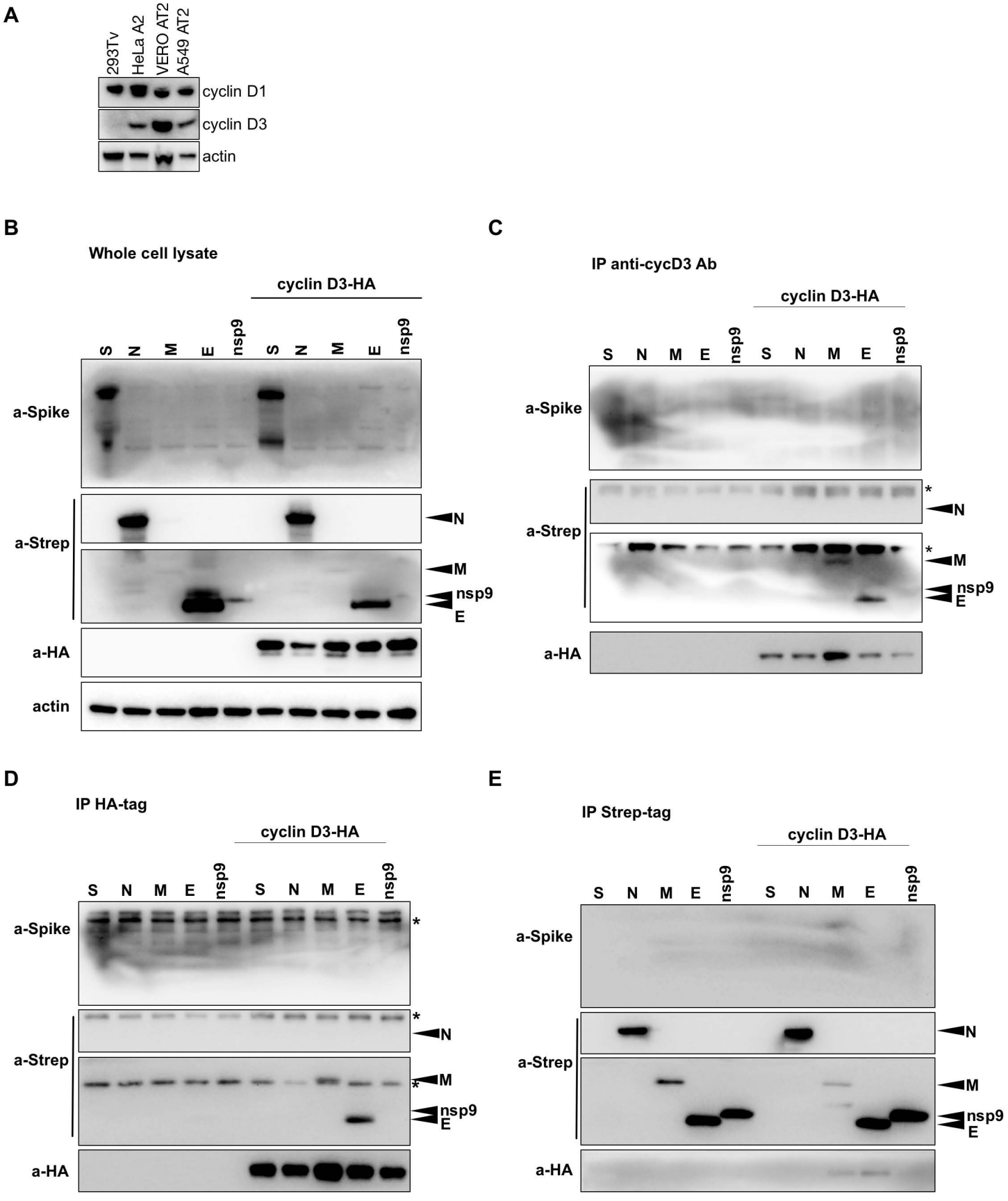
A
293Tv
HeLa A2
VERO AT2
A549 AT2
cyclin D1
cyclin D3
actin
B
Whole cell lysate
cyclin D3-HA
S N M E nsp9 S N M E nsp9
a-Spike
a-Strep
N
M
nsp9
E
a-HA
actin
C
IP anti-cycD3 Ab
cyclin D3-HA
S N M E nsp9 S N M E nsp9
a-Spike
a-Strep
*
N
*
M
nsp9
E
a-HA
D
IP HA-tag
cyclin D3-HA
S N M E nsp9 S N M E nsp9
a-Spike
*
a-Strep
*
N
*
M
nsp9
E
a-HA
E
IP Strep-tag
cyclin D3-HA
S N M E nsp9 S N M E nsp9
a-Spike
a-Strep
N
M
nsp9
E
a-HA

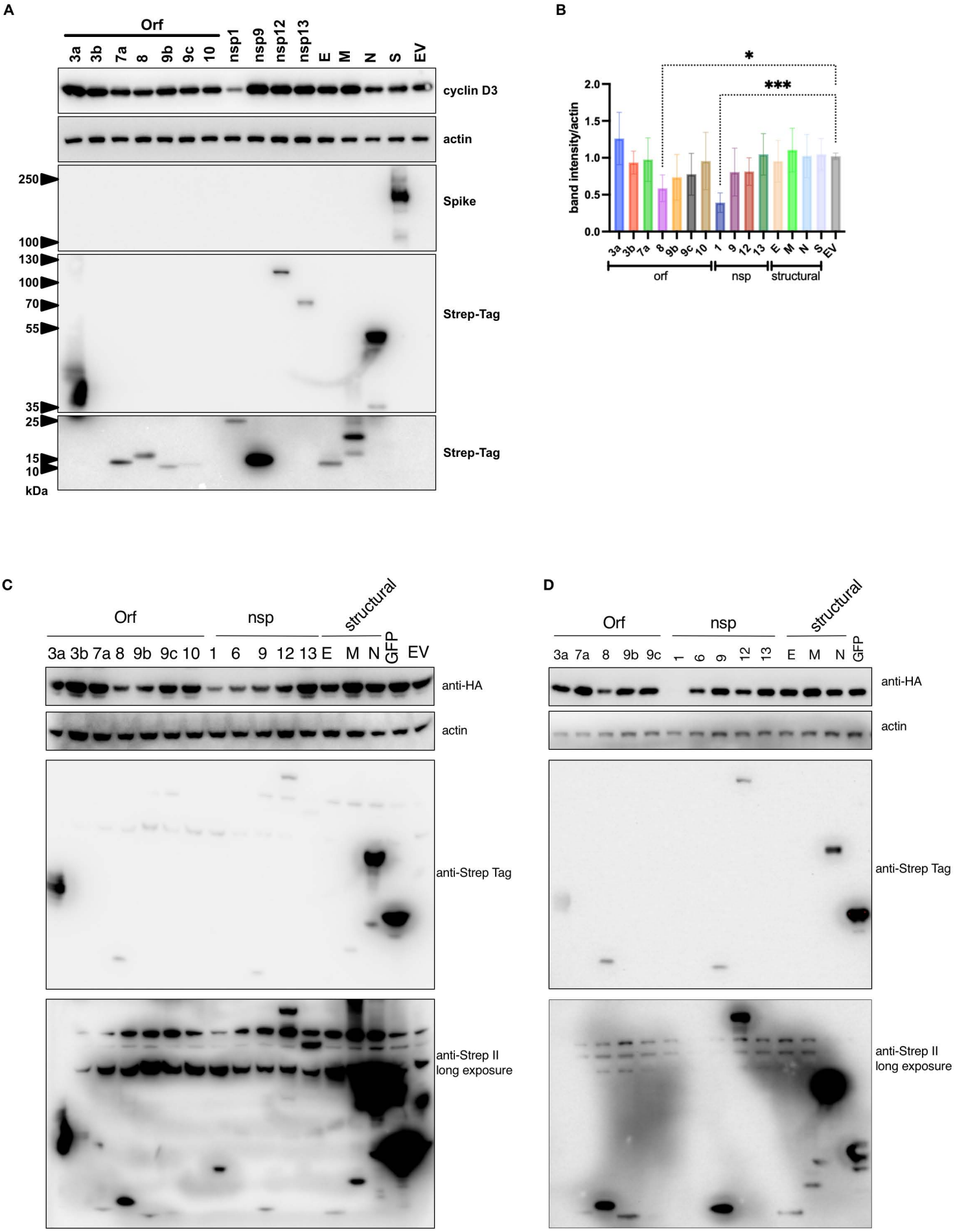
A
Orf
3a 3b 7a 8 9b 9c 10 nsp1 nsp9 nsp12 nsp13 E M N S EV
cyclin D3
actin
250
100
Spike
130
100
70
55
35
Strep-Tag
25
15
10
kDa
Strep-Tag
B
band intensity/actin
2.0
1.5
1.0
0.5
0.0
*
***
3a 3b 7a 8 9b 9c 10 1 9 12 13 E M N S EV
orf
nsp
structural
C
Orf
nsp
structural
3a 3b 7a 8 9b 9c 10 1 6 9 12 13 E M N GFP EV
anti-HA
actin
anti-Strep Tag
anti-Strep II
long exposure
D
Orf
nsp
structural
3a 7a 8 9b 9c 1 6 9 12 13 E M N GFP
anti-HA
actin
anti-Strep Tag
anti-Strep II
long exposure